



Multi-vehicle cooperation and nearly fuel-optimal flock guidance in strong background flows



Zhuoyuan Song^{a,c}, Doug Lipinski^{a,c}, Kamran Mohseni^{a,b,c,*}

^a Department of Mechanical and Aerospace Engineering, University of Florida, Gainesville, FL, USA

^b Department of Electrical and Computer Engineering, University of Florida, Gainesville, FL, USA

^c Institute for Networked Autonomous Systems, University of Florida, Gainesville, FL, USA

ARTICLE INFO

Keywords:

Multi-vehicle control
Flocking
Underwater vehicle
Ocean current
Guidance

ABSTRACT

A multi-vehicle flocking and guidance control scheme is proposed for small autonomous underwater vehicles in the presence of strong ocean flows that exceed vehicles' actuation capabilities. The flocking problem and flock guidance problem are simultaneously addressed by enduing fluid properties to the vehicle swarm. This control scheme generates cohesive flocking behavior with inherent inter-vehicle collision avoidance and velocity consensus. The vehicle flock is guided along a fuel-optimal trajectory calculated for an individual vehicle based on background flow predictions, allowing us to compute a single optimal trajectory while still achieving robust flocking performance and near optimality for all vehicles. Resultant vehicle trajectories are nearly fuel-optimal when the spatial variation of background flow velocities across the flock is small. Dimensional analysis uncovers two important independent parameters dictating the balance between swarm compressibility and the degree of velocity consensus. The efficiency of the presented method is demonstrated in simulations with two synthetic background flow fields resembling realistic ocean flow patterns, and a flow field reconstructed based on ocean model data. A quantitative comparison with a generic artificial potential based control scheme shows that, owing to the inherent velocity consensus effect, the proposed method results in better flocking behavior and less actuation energy consumption.

1. Introduction

The emergent behaviors of schooling, swarming, and flocking, often observed as the collective behavior of swarms of biological organisms including schooling fish (Cullen et al., 1965; Morrow, 1948) or flocking birds (Major and Dill, 1978), have long been a topic of research. A considerable amount of effort has been made on identifying rules governing swarm behavior (Reynolds, 1987), analyzing the stability and convergence of resultant flocking motion (Gazi and Passino, 2003; Toner and Tu, 1998), and applying such findings to control problems in robotics (Kelley and Ouellette, 2013; Rubenstein et al., 2014; Shang and Bouffanais, 2014).

At the most fundamental level, flocking requires three key elements: *separation*, *cohesion*, and *alignment* (Reynolds, 1987). The first element, separation, involves maintaining a necessary spacing between adjacent agents to avoid inter-agent collisions. The second element, cohesion, involves agents staying in some neighborhood of each other, or, alternatively, staying close to the centroid of the flock. The final element, alignment, involves the agents matching the velocities of their neighbors to give rise to directional flock movements.

These qualitative flocking rules can be satisfied by a variety of approaches, and many additional considerations can be added including individual agent motion and vision constraints. Specific implementations of flocking algorithms have also been analyzed to show convergence and stability of the resulting flocks (Jadbabaie et al., 2003; Olfati-Saber, 2006).

Robot flock guidance is of great importance to many multi-robot applications such as vehicle fleet transportation (Çelikkanat and Şahin, 2010). Compared with the single-robot counterpart, multi-robot guidance adds more complexity, which is mainly due to the potential interactions among robots, as well as between robots and the working environment. The situation is even worse when there exist dominating environmental forces that exceed robots' actuation capabilities.

Autonomous robots, especially micro/miniature aerial vehicles (MAVs) and small-scale autonomous underwater vehicles (AUVs), are usually small in size and weight with limited on-board actuation, power, memory, communication, and processing capabilities, in order to achieve low costs and fast turnaround. These platforms are therefore susceptible to strong gusts or ocean currents, respectively, and they are not capable enough to move against the background flow in order to

* Corresponding author.

E-mail address: mohseni@ufl.edu (K. Mohseni).

follow arbitrarily designated trajectories. There are even situations where certain regions of the domain may not be accessible due to high-speed background flows. Conventionally, for large aircraft or marine vessels, the impact of background flows on vehicle motion is simply considered as small disturbances, and the vehicles of interest are assumed to have sufficient actuation capabilities to “fight” against the flows (Fossen and Sagatun, 1991). However, when the velocity magnitudes of the background flows are comparable to or larger than vehicles’ maximum speeds, it is essential that the path planning method exploits background flow knowledge whenever possible.

For a single vehicle, such an optimization problem may be approximately solved relatively easily. Assuming that a good forecast of the background velocity field is available, many techniques exist that are capable of generating an optimal trajectory between two points (Inanc et al., 2005; Kim and Ura, 2003; Kruger et al., 2007; Petres et al., 2007; Rhoads et al., 2010; Witt and Dunbabin, 2008). However, as the number of vehicles increases, it becomes computationally impractical to calculate the optimal trajectories for all vehicles and avoid inter-vehicle collisions at the same time. In addition, when multi-vehicle flocking is considered, the problem quickly becomes intractable due to potential interactions among vehicles and the constraints required to maintain safe inter-vehicle spacings to avoid collisions. Multiple existing techniques have been presented for flock control related problems, the most popular of which include flocking, formation control, and hierarchical cooperation control (Barca and Sekercioglu, 2013; Brambilla et al., 2013; Ren et al., 2005). With few exceptions (DeVries and Paley, 2012; Lipinski and Mohseni, 2011), these techniques do not account for large background flow fields. Therefore, an ideal multi-vehicle flocking and flock guidance algorithm should allow us to compute just a single optimal trajectory while still achieving robust flocking performance and near optimality for all vehicles.

In this paper, a multi-vehicle control method is proposed that combines both vehicle flocking control and flock guidance. We focus on the realization of multi-AUV collaborative control and guidance in the presence of strong ocean currents, during which the swarm cohesion is maintained. The flock guidance algorithm guarantees that actuation fuel consumption of the entire flock is nearly optimal, which is critical for AUV applications. This is achieved through utilizing knowledge of the ocean current velocity field, which may be estimated by ocean general circulation models (OGCMs) such as Hybrid Coordinate Ocean Model (HYCOM) (Chassignet et al., 2009) and Regional Ocean Modeling System (ROMS) (Shchepetkin and McWilliams, 2005). This distributed flock control algorithm requires solely local measurement and communication in a confined neighborhood of each agent to achieve fluid-like flocking motion. As a result, requirements for cohesion, inter-vehicle collision avoidance, and alignment are naturally satisfied.

In our proposed technique, a fuel-optimal trajectory is computed for a single vehicle within a domain with strong and spatiotemporally changing background flows. Given such a trajectory, a swarm of vehicles may be guided along the trajectory with the center of the swarm approximately following the truly optimal trajectory. Multi-vehicle path following in changing background flow fields requires special treatment due to the dependency of swarm dynamics on ocean flow dynamics. This is addressed by making the vehicle swarm move and deform like a fluid. It provides us with an analogy that guides our control and understanding of the vehicle flock behavior based on our physical intuition:

- fluid compressibility \Leftrightarrow flock compressibility;
- fluid viscosity \Leftrightarrow velocity consensus.

This vehicle flock control and guidance method results in nearly fuel-optimal trajectories for each vehicle in the swarm given that the background flow velocity gradients experienced by the swarm are small.

We present detailed methodologies and theories for the fluid-based, multi-vehicle control and guidance scheme (Lipinski and Mohseni, 2013). The maximum and average energy usage per vehicle are analyzed through extensive simulations to verify the feasibility of the proposed method in real-world applications. We also derive relationships for how the total fuel cost scales with the flock size and provide guidelines for parameter selection given certain desired performance. Dimensional analysis over the multi-vehicle control law discovers two important independent variables that dictate the resultant flocking behavior. To demonstrate the importance of swarm viscosity to the flocking performance, the proposed control scheme is compared quantitatively with an artificial potential based control scheme. Owing to the inherent velocity consensus effect, our multi-vehicle cooperation and guidance method performs better in terms of both flocking performance and energy consumption.

The rest of this paper is organized as follows. In Section 2, we discuss some related works on multi-vehicle control and the recent progress in underwater vehicle studies in strong currents. Section 3 formulates the problem and briefly includes the fundamental preliminaries on multi-vehicle control using fluid properties. The stability of this control scheme is then discussed, followed by a dimensional analysis of our control algorithm. The optimal trajectory generating method is outlined in Section 4 with a theoretical analysis of the sub-optimality of vehicles’ actuation costs. Section 5 presents validation results of the proposed control scheme in both artificial background flow fields resembling real ocean flows and a simulated flow field of the Gulf of Mexico reconstructed from ocean current model data sets. A quantitative comparison between our approach and the generic, potential function based approach is presented in Section 6. Finally, we conclude the paper in Section 7.

2. Related works

Compared with the vast majority of swarm robotic applications, underwater robot flocking is a relatively new research topic. Collaboration among multiple AUVs has proven beneficial for improving task efficiency as well as sensing coverage. Unlike most ground robot flocking applications, the unique nature of the chaotic underwater environment imposes numerous constraints on the development of flocking strategies for underwater platforms. The presence of turbulence in ocean flows requires extra care while analyzing vehicle dynamics such that these environmental impacts are properly considered (Fossen, 2011; Thomasson and Woolsey, 2013).

To this end, some endeavors have been made to address a wide range of practical problems using collaborating underwater robots (Paley et al., 2008; Zhang et al., 2007). For instance, Leonard et al. (2007) investigated the path-planning problem for an underwater glider fleet in the presence of ocean currents. Optimal sampling performance was achieved by navigating along paths minimizing the model estimation error of the sampled field. As another example, Paley (2007) discussed the cooperative control of an underwater vehicle fleet under the influence of a steady, uniform flow. A feedback control law was designed to maintain proper spacings between two gliders on a circular track. Caruso et al. (2008) analyzed the impact of ocean flows on the mobility of an underwater sensor swarm in terms of connectivity, localization performance, and coverage. It was shown that, in a meandering jet, a multiple-deployment process improves the connectivity lifetime of the sensor network. More recently, Mallory et al. (2013) studied the allocation of a swarm of homogeneous mobile sensors in gyre flows through tracking the Lagrangian coherent structure (LCS). Based on the knowledge of the LCS map, segmented by maximum finite-time Lyapunov exponent (FTLE) ridges, agent-level control laws were designed to determine whether a given agent should stay or leave the current segment in an auction-actuation fashion.

On-board power constraint is a major limitation of AUVs in long-term applications such as ocean monitoring and data collection. Therefore, it is crucial that the significance of ocean currents is properly recognized and

utilized instead of being treated as small disturbances. To this end, several vehicle guidance algorithms have been proposed to remedy these environmental impacts on the motions of small-scale AUVs (Lermusiaux et al., 2016; Lipinski and Mohseni, 2011). Inanc et al. (2005) proposed an optimal trajectory generation strategy for underwater gliders in ocean flows. They utilized ocean flow forecasts in the context of LCS to optimize the fleet travel time. Lolla et al. (2012) also proposed a time-optimal path planning strategy using level set methods that evolve a waterfront, formed by a set of particles representing multiple realizations of a vehicle, from the starting point to the goal location. The optimal path was obtained through backtracking the particle arriving at the target location. Each vehicle's path was computed individually. In Lipinski and Mohseni (2011), an optimal guidance algorithm was proposed for a vehicle fleet in order to minimize the actuation energy through utilizing the background flow whenever possible.

Meanwhile, the past few decades have witnessed tremendous advance in the field of swarm robotics and the collective motion of autonomous robots. Multiple recent reviews can be found on several related topics such as the collective motion observed in nature and the corresponding robotic realizations (Vicsek and Zafeiris, 2012), methodologies and theories in swarm robotics (Barca and Sekercioglu, 2013; Brambilla et al., 2013), distributed multi-robot collaboration and decision making (Cao et al., 2013; Sabattini et al., 2013), etc. Among the existing swarm control methods, we are particularly interested in those that encode fundamental physical laws. Such methods usually introduce extra controllability to the flock. As well, our physical intuition can help us in understanding the resultant flocking behavior. Hsieh and Kumar (2006) presented a pattern generation strategy through controlling a swarm of ground robots with a virtual interacting force law and a potential function that determines the final shape of the swarm. Inspired by their work, Pimenta et al. (2008) proposed a swarm control strategy using smoothed particle hydrodynamics (SPH) instead. They conducted a series of experiments with seven ground robots in an environment with static obstacles. This work was then extended to address moving obstacles (Pimenta et al., 2013). Shaw and Mohseni (2011) also presented an SPH-based, cooperative control method for multiple unmanned aerial vehicles (UAVs). The proposed algorithm was tested in a series of experiments using low-cost, Delta-wing UAVs to help with the wireless communication characterization.

Unlike ground robot applications, underwater vehicles' flocking motions are closely coupled with the background flow dynamics. Instead of merely considering interactions among flock agents using abstraction methods, we endow generic fluid properties to the AUV flock. To the best of the authors' knowledge, modeling and controlling swarms of underwater vehicles as fluids interacting with a background flow are novel to the field. The resulting motions of the vehicle swarms share similar characteristics with the surrounding fluid flows, making our approach more natural than other abstraction-based, multi-vehicle control schemes in dealing with swarm movements in a fluid background. When handling the realization of the cooperative control in this study, we focus on the fundamental physical interpretations of the resultant flocking properties. We emphasize the importance of the macroscopic, fluid-like characteristics of an emergent vehicle flock. These characteristics are determined by two non-dimensional numbers widely used in fluid characterizations: the Mach number M and the Reynolds number Re , which are less recognized in the robotics community. To elaborate their significance to a broader audience, we explain the physical intuitions behind both of the non-dimensional numbers, and relate them to corresponding emergent properties of a vehicle flock. In addition, a non-dimensionalized formulation of the cooperative control law is presented for the first time to guide the parameter selection in the design of a multi-vehicle control algorithm that leads to a balance between flock morphology¹ and velocity consensus.

¹ By morphology, we mean that the shape of the flock and the topology of inter-agent communication are subject to changes.

3. Multi-vehicle control and flock guidance

Multi-agent flocking control using physical abstraction is commonly achieved through applying artificial potential functions between adjacent agents to mimic interactions between atoms or molecules. The Lennard-Jones potential and the gravitational potential are usually adopted due to their simple mathematical representations and satisfactory performance in many applications (Spears et al., 2005; Spears and Spears, 2012), most of which are ground robot applications. When large environmental forces affect agents' motions, a more sophisticated strategy is desired to increase flocking robustness.

Our multi-vehicle cooperation and flock guidance algorithm is built upon the SPH framework. The SPH method is a Lagrangian, mesh-free discretization of the Navier-Stokes equations that govern fluid motions. It was originally introduced for modeling astrophysical phenomena, and then extended to continuous solid and fluid mechanics (Gingold and Monaghan, 1977; Lucy, 1977). In a cooperative vehicle control context, each vehicle can be treated as an individual fluid particle with imaginary physical properties such as size, mass, and viscosity. Vehicle interactions were handled in a low-level scheme where imaginary inter-vehicle forces are considered. A high-level control scheme dictates the general swarm behavior through adjusting the emergent, macroscopic fluid properties.

To the best of our knowledge, the first implementation of SPH in robotic swarm control was reported by Perkinson and Shafai (2005), who studied a sensor coverage problem with obstacle avoidance using SPH to generate local control for a robot swarm. Later, Pac et al. (2007) developed a two-level robot swarm control scheme using SPH to accomplish missions including robot swarm deployment, dispatching, and flocking. Many other previous works have also used SPH in a cooperative control context for different applications with generally good results (Huhn and Mohseni, 2009; Lipinski and Mohseni, 2010; Pimenta et al., 2008, 2013; Shaw and Mohseni, 2011; Zhao et al., 2011). In many ways, SPH control is similar to control using artificial potential fields. However, since SPH provides a complete description of fluid dynamics, it includes more properties that are beneficial to multi-vehicle control problems. For instance, SPH includes viscous forces that provide velocity consensus effect, which would need to be added to other artificial potential based control schemes. Additionally, with similar force-distance potentials, the density variable in the SPH-based control scheme provides more consistent inter-vehicle spacing control than artificial potential based control schemes.

We favor the abstraction method based on SPH mainly due to three reasons. Firstly, SPH is a complete description of a continuous fluid, the same medium that vehicles operate in. It inherently comprises both inter-agent attraction and repulsion as the Lennard-Jones potential and the gravitational potential. In addition, SPH introduces the viscous effect in a fluid into vehicle flocking, which results in desirable inter-vehicle velocity consensus. Most importantly, as a successful method for computational fluid dynamics, SPH can be used to compute the evolution of the background flow. Applying the same method in multi-vehicle control is beneficial to future studies on the coupling between flow dynamics and vehicle flock dynamics.

In this section, we include some SPH preliminaries for the convenience of the reader. The selection of appropriate parameters based on the scales of the problem is also discussed. The stability of the resultant vehicle control law is analyzed using Lyapunov stability theory. Dimensional analysis is performed to uncover the fundamental relationship between flock performance and two key independent variables, providing a convenient parameter selection guideline.

The basic concept of this approach is to have the vehicle swarm behave like a continuous fluid. Fluid properties are applied through particle discretization using a smoothing kernel, which governs the interactions among adjacent agents. The equations of agents' motion are determined by conservation laws of mass and momentum. These conservation laws act to prevent collisions between agents since two

fluid particles cannot occupy the same location in space at the same time. Obstacle avoidance is also naturally embedded relying on the fact that fluids cannot penetrate solid obstacles. However, we only focus on inter-vehicle collision avoidance in this paper since collisions with obstacles are much less likely than inter-vehicle collisions in long-distance vehicle swarm guidance in open ocean. Interested readers are referred to Shaw and Mohseni (2011) and Pimenta et al. (2013) for obstacle avoidance using SPH-based approaches. When a compactly supported kernel function is chosen, the range of agent interactions is limited such that the resultant control scheme can be implemented as a distributed computation that requires little processing power. From a flock control perspective, this enables a distributed control scheme where only local sensing and communication are required, which is critical to underwater applications where sensing and communication are usually constrained.

It is helpful to first give a high-level overview of the basic SPH equations of fluid motion and discuss how they can be applied to cooperative control problems. For additional details, the reader is referred to Liu and Liu (2003) or Monaghan (1992, 2005, 2012) and the references therein.

3.1. Preliminaries on fluid dynamics and its discretization

The SPH discretization relies on a smoothing kernel, through which the fluid properties are applied. The kernel should be normalized and, ideally, compactly supported for computational efficiency. Therefore, the states of each particle only depend on information in the close vicinity. This motivates us to choose spline-based kernel functions over others, including Gaussian kernel functions that do not have compact support, and will encumber the scalability of the control algorithm. The following two different kernels are used in this study:

$$W_1(\vec{r}_{ij}, h_{ij}) = \frac{C_1}{h_{ij}^d} \begin{cases} s^2 - 4s + 4 & \text{if } s \leq 2 \\ 0 & \text{if } s > 2 \end{cases} \quad (1)$$

and

$$W_2(\vec{r}_{ij}, h_{ij}) = \frac{C_2}{h_{ij}^d} \begin{cases} 4 - 6s^2 + 3s^3 & \text{if } 0 \leq s \leq 1 \\ (2-s)^3 & \text{if } 1 < s \leq 2 \\ 0 & \text{if } s > 2 \end{cases} \quad (2)$$

Here index i and j denote particle identities, d is the dimension of the problem, and h_{ij} is the smoothing width, taken here to be $\max(h_i, h_j)$ if two particles have different smoothing widths. The function variable s is defined as $s = \|\vec{r}_{ij}\|/h_{ij}$ with $\vec{r}_{ij} = \vec{r}_i - \vec{r}_j$ being the relative position vector from particle i to particle j . Coefficients C_1 and C_2 are normalization constants such that $\int W_1 d\vec{x} = \int W_2 d\vec{x} = 1$. In a two-dimensional case ($d = 2$), these values can be calculated as $C_1 = 3/(8\pi)$ and $C_2 = 5/(14\pi)$. In the case with only a single group of vehicles, all vehicles can be assigned with the same h value for simplification. And the value of h depends on actual sensor and communication ranges. We will discuss the usage of virtual particles for flock guidance, which typically have a larger smoothing length. The kernel functions are plotted in Fig. 1. Since both kernels are compactly supported, the ranges of agent interactions are limited. This enhances computational efficiency ($O(n)$ for n particles) and implementation simplicity.

Both W_1 and W_2 are kernel functions with compact support. The major difference between them is that W_2 has a zero gradient at the origin. Kernel W_1 is a second-order spline kernel function that is suitable for vehicle-vehicle interactions. It creates large repelling forces between agents that are too close to each other to provide robust inter-vehicle collision avoidance. Kernel W_2 , on the other hand, is a cubic spline kernel function that will be used for flock guidance. It has zero gradient at the origin, making it suitable for a virtual attracting vehicle. Since the guidance forces are proportional to the kernel gradient, this kernel prevents large guidance oscillations for nearby vehicles.

A complete description of fluid dynamics includes the conservation

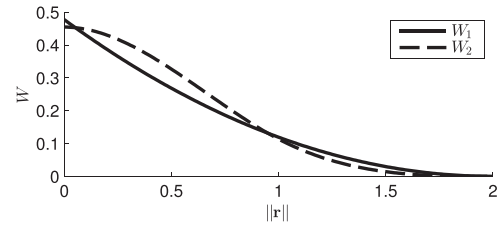


Fig. 1. The SPH smoothing kernels used in this study for $h = 1$. Kernel W_1 is used for vehicle-vehicle interactions and kernel W_2 is used for flock guidance.

of mass, momentum, and energy, as well as an *equation of state* that relates density, temperature, and pressure. SPH discretizes continuous fluid properties into individual particles through aforementioned kernel functions. Such an approximation scheme is known to have second-order accuracy or h^2 accuracy (Liu and Liu, 2003; Monaghan, 1992). Under such a discretization scheme, the particle density equation and the conservation of momentum equation can be derived from the Navier-Stokes equations as

$$\rho_i = \sum_j W(\vec{r}_{ij}, h) m_j, \quad (3)$$

$$\frac{d\vec{v}_i}{dt} = - \sum_j m_j \left(\frac{P_i}{\rho_i^2} + \frac{P_j}{\rho_j^2} \right) \nabla_i W(\vec{r}_{ij}, h) + \sum_j m_j \frac{2\mu}{\rho_i \rho_j} \frac{\vec{v}_{ij}}{\|\vec{r}_{ij}\|} \frac{dW}{d\|\vec{r}_{ij}\|}, \quad (4)$$

for density ρ , mass m , pressure P , and viscosity coefficient μ . The velocity vector is the time derivative of the position vector, $\vec{v}_i = \dot{\vec{r}}_i$. Operator ∇_i represents the gradient with respect to the coordinates of particle i , and the relative velocity between two different particles is $\vec{v}_{ij} = \vec{v}_i - \vec{v}_j$. It is worth mentioning that the conservation of energy is typically also required for a complete fluid system description. We did not include it here since it can be decoupled from the conservation of momentum and does not play a role in our flock control scheme where heat conduction is not considered. Interested readers are referred to Monaghan (1992) or Liu and Liu (2003) for a complete derivation.

The first term on the right-hand side of (4) represents the pressure force per unit mass resulting from the pressure and density gradients. It acts as an attractive or repulsive force between interacting agents. The second term is the artificial viscosity that represents the shear stress in flows. Unlike the artificial viscosity adopted by Pimenta et al. (2013), which was from Monaghan (1992) and first introduced by Benz (1990) to permit the modeling of strong shocks, we employ a more realistic form used by Morris et al. (1997). This form has proven more accurate and appropriate for low flow velocities that are considered in this work.

By applying a kernel approximation scheme, the discretized pressure P_i is computed through an *equation of state* suggested by Monaghan (1994)

$$P_i = B \left[\left(\frac{\rho_i}{\rho_0} \right)^\gamma - 1 \right], \quad (5)$$

where B is the bulk modulus representing the compressibility of the fluid, and γ is a constant depending on the type of fluid being simulated (usually $\gamma = 7$ for water). The bulk modulus is defined as $B := -VdP/dV$ with V being the volume. ρ_0 is the reference density that can be arbitrarily chosen to control the desired natural particle spacing. In practice, B can be calculated through $B = c^2 \rho_0$, where c is the speed of sound in the fluid of interest. When the maximum agent speed (flow speed) $\|\vec{v}\|_{\max}$ is known, the Mach number M can be calculated through $M = \|\vec{v}\|_{\max}/c$. As we will show later, M is a very important non-dimensional number dictating the compressibility of the fluid. For simulating quasi-incompressible fluids, M can be set to a small number (usually 0.1–0.01) to make the swarm behave as incompressible flows. In this case, further simplification can be achieved by setting $\gamma = 1$ without noticeable changes in performance.

The behavior of the multi-vehicle cooperative control system also relies on the selection of μ and m_i . In a cooperative control context, these parameters should be determined based on the capabilities of the agents and the desired flock behavior. We will present a guideline for selecting these parameters in the following paragraphs.

We start by specifying that agent-agent interactions should use kernel W_1 . Since magnitudes of W_1 and ∇W_1 increase monotonically as $\|\vec{r}_{ij}\| \rightarrow 0$, the repulsive pressure force between agents will increase monotonically as agents approach each other, which leads to good inter-agent collision avoidance performance. Note that the pressure force terms in (4) act in line with ∇W to generate purely attracting or repelling forces between particles depending on the sign of P .

We then determine an appropriate value for m_i . Note that when $\rho_i < \rho_0$, the pressure P_i is negative, which leads to attracting forces between agents. As two particles approach each other, their densities increase according to (3). So in isolation, two agents will experience only repulsive forces if $m_i \geq \rho_0/W(\vec{0}, h_{ij})$ and only attracting forces (meaning they will likely collide) if $m_i \leq \rho_0/(2W(\vec{0}, h_{ij}))$. To create a long-range attraction and a short-range repulsion, we set

$$m_i = \frac{2}{3} \frac{\rho_0}{W(\vec{0}, h_{ij})}. \tag{6}$$

The resulting pressure forces between vehicles are shown in Fig. 2 for $h = 1$ and $c = 1$. A long-range attractive force region and a short-range repulsive force region are created with a stable equilibrium at $\|\vec{r}\|/h = r^* \approx 0.5858$.

To determine the appropriate values for μ and c , we analyze the interactions between two agents with $\|\vec{v}_{ij}\| = v_{\max}$, where v_{\max} is the maximum agent speed and $\|\vec{r}_{ij}\| = h_{ij}r^*$. In this case, each of the vehicles will have the same density and pressure values of

$$\rho = \frac{2\rho_0}{3} \left(1 + \frac{W_1(\vec{r}_{ij}, h_{ij})}{W_1(\vec{0}, h_{ij})} \right), \tag{7}$$

and

$$P = B \left(\frac{\rho}{\rho_0} - 1 \right), \tag{8}$$

leading to a pressure force (per unit mass) of

$$\|F_P\| = \left| \frac{2mP}{\rho^2} \nabla W_1(\vec{r}_{ij}, h_{ij}) \right|, \tag{9}$$

and a viscous force (per unit mass) of

$$\|F_\mu\| = \mu \left| \frac{2mv_{\max}}{\rho^2 \vec{r}_{ij}} \frac{dW_1(\vec{r}_{ij}, h_{ij})}{d\|\vec{r}_{ij}\|} \right|. \tag{10}$$

The viscous force acts in opposition to the velocity difference between agents and therefore behaves as a consensus or velocity matching term. The relative strength of the pressure and the viscous forces dictates the trade-off between collision avoidance and velocity consensus in the SPH control scheme. This can be quantified with a ratio Φ of two non-

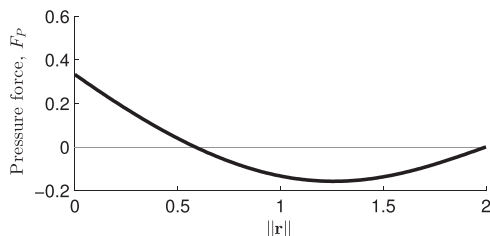


Fig. 2. The SPH pressure force between two isolated vehicles using $m = 2\rho_0/(3W(\vec{0}, h_{ij}))$, $h = 1$, and $c = 1$. It consists of a long-range attractive region and a short-range repulsive region with a stable equilibrium spacing of $\|\vec{r}\|/h = r^* \approx 0.5858$.

dimensional parameters, Reynolds number Re and Mach number M , as

$$\Phi = \frac{Re}{M^2} = \frac{\|F_P\|}{\|F_\mu\|}, \tag{11}$$

with Re and M being important independent parameters characterizing fluid properties and regimes, which will be discussed in detail later in Section 3.3. This relationship provides an intuitive guidance for the performance of the vehicle swarm during the design of a control algorithm.

The motion of autonomous vehicles, especially underwater vehicles, is usually subject to multiple realistic constraints. Vehicles designed by our group are equipped with novel, bio-inspired vortex ring actuators such that control surfaces are not needed, and improved maneuverability can be achieved (Krieg and Mohseni, 2010). These thrusters generate trusts by expelling finite jets of water periodically, mimicking the local motion of jellyfish, squid, octopus, and other cephalopods, to provide maneuvering forces (Krieg and Mohseni, 2015). They have demonstrated faster time-response compared to propeller thrusters in reaching their peak thrust output, which is crucial in minimizing the actuation delay during the implementation of a cooperative control algorithm on underwater vehicles (Krieg et al., 2011; Song et al., 2016). Unlike most conventional underwater vehicles, this design provides low-drag vehicle profile and high maneuverability in all degrees of freedom except for roll. In a more general case with 2D planar motion, constraints on the minimum turning radius and the maximum forward speed need to be considered, giving a way to set the values of c and μ . If the minimum turning radius of the agents is R_{\min} , the associated centripetal acceleration is $a = v_{\max}^2/R_{\min}$. To set the total force magnitude to an appropriate scale, we let

$$\frac{v_{\max}^2}{R_{\min}} = \|F_P\|. \tag{12}$$

Thus, choosing a desired force ratio Φ and knowing the agents' maximum speed v_{\max} and minimum turning radius R_{\min} allow us to determine c and μ using (11) and (12).

Flock guidance is handled through the use of reduced-density, virtual particles. Based on (5), low-density (and therefore low-pressure) particles experience attracting forces. This is analogous to pressure gradients in fluid flows that drive fluid to low pressure regions. We use the second smoothing kernel W_2 for these virtual particles. Having large forces near the virtual attracting particle, as produced by W_1 , can lead to rapid oscillations. Kernel W_2 generates zero force in close proximity to virtual particles since $\nabla W_2(\vec{0}, h_{ij}) = 0$, helping to limit oscillations. For additional simplification without loss of generality, we apply the zero-density limit and eliminate viscosity for these virtual attracting particles, since commonly only one virtual particle is required for each vehicle flock. This results in an attracting force (per unit mass) on the agents of

$$\|F_i\| = \left| \frac{c_a^2}{W_2(\vec{0}, h_{ij})} \nabla_i W_2(\vec{r}_{ij}, h_{ij}) \right|. \tag{13}$$

This force is always toward the virtual particle and its plot is presented in Fig. 3. The speed of sound c_a for the virtual attracting particles is determined such that the acceleration caused by the attracting particles is half of the maximum vehicle acceleration based on the minimum turning radius, which leaves agents enough remaining actuation authorities for flocking activities. This means that the virtual attracting particles have

$$c_a = \sqrt{\frac{h_{ij}v_{\max}^2}{6R_{\min}}}. \tag{14}$$

With all relevant parameters for the proposed control equations determined, the cooperative control algorithm computes the desired

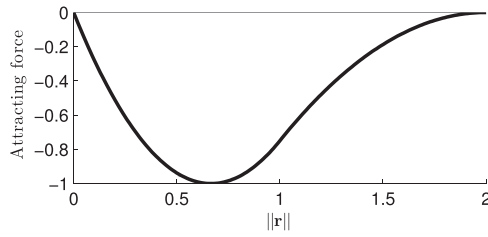


Fig. 3. The SPH attracting force from a reduced density virtual particle using $h = 1$, $c = 1$, and kernel w_2 .

acceleration for each agent. For a given vehicle, the interactions with all neighbors ($\|\vec{r}_{ij}\| < 2h_{ij}$) are considered, and a small artificial drag force is added such that the vehicle will eventually come to rest in the absence of external interactions. The complete dynamics for an individual vehicle i in a fleet consisting of a total number of N vehicles can be described as

$$\frac{d\vec{r}_i}{dt} = \vec{v}_i, \quad (15)$$

$$\frac{d\rho_i}{dt} = \sum_{j=1}^N m_j (\vec{v}_i - \vec{v}_j) \nabla_i W(\vec{r}_{ij}, h), \quad (16)$$

$$\frac{d\vec{v}_i}{dt} = - \sum_{j=1}^N m_j \left(\frac{P_i}{\rho_i^2} + \frac{P_j}{\rho_j^2} \right) \nabla_i W(\vec{r}_{ij}, h) + \sum_{j=1}^N m_j \frac{2\mu}{\rho_i \rho_j} \frac{\vec{v}_{ij}}{\|\vec{r}_{ij}\|} \frac{dW}{d\|\vec{r}_{ij}\|} - \varepsilon \vec{v}_i, \quad (17)$$

where ε is the artificial drag coefficient, and we use $\varepsilon = 0.05$ in this paper. It should be noted that, although the summation is over all N agents, only adjacent neighbors in the smoothing length will actually be involved in the calculation of the control decisions for each vehicle. This makes our flock control and guidance method distributed and scalable. Additionally, a constraint function is applied that limits the velocity and acceleration to achievable levels. The evolution equation for the agents is therefore

$$\ddot{\vec{x}}_i = \text{constrain} \left(\frac{d\vec{v}_i}{dt} \right). \quad (18)$$

It is worth mentioning that the agent dynamics described by (15)–(17) treat each mobile agent as a point mass and they do not explicitly address the low-level, background flow-agent interactions during the implementation of this control law on actual vehicles. Low-level vehicle control under potential impacts from the background flow is beyond the scope of this work. Interested readers are referred to [Xu and Mohseni \(2014\)](#) on a nonlinear trajectory-following strategy for autonomous underwater vehicles using feed-forward signal from a bio-inspired lateral-line sensory system.

3.2. Stability analysis

The stability of a multi-vehicle cooperative control system is crucial to the implementation of the designed control policies. For an unstable system, unpredicted motions of individual agents may lead to control failures of the entire fleet. In an underwater vehicle cooperation context, instability usually causes extra cost in control energy and travel time.

Proposition 1. *Given a multi-agent system of which the agent dynamics can be described by (15)–(17) and the agents stay connected, there exist system equilibrium states that satisfy $(\rho_i = \rho_0, \vec{v}_i = 0) \forall i = 1, \dots, N$.*

Proof. When the system is at the equilibrium states, for each agent in the system, there are $d\vec{r}_i/dt = 0$, $d\rho_i/dt = 0$, and $d\vec{v}_i/dt = 0$. The condition $d\rho_i/dt = 0$ is trivially satisfied when $d\vec{r}_i/dt = 0 \forall$

$i = 1, \dots, N$. In (17), a necessary condition for $d\vec{v}_i/dt = 0$ is

$$\frac{P_i}{\rho_i^2} + \frac{P_j}{\rho_j^2} = 0,$$

to which there exists a solution $\rho_i = \rho_j = \rho_0$ based on the equation of state (5). \square

To investigate the stability of this system equilibrium trajectory, we analyze the positive definite Lyapunov candidate function

$$V = \frac{1}{2} \sum_i \vec{v}_i^T \vec{v}_i + \sum_i e_i, \quad (19)$$

where $\sum_i e_i$ is the system energy due to conservative forces, and its time derivative for a single agent can be expressed as

$$\dot{e}_i = \frac{1}{2} \sum_i m \left(\frac{P_i}{\rho_i^2} + \frac{P_j}{\rho_j^2} \right) \vec{v}_{ij}^T \nabla_i W(\vec{r}_{ij}, h). \quad (20)$$

It is worth mentioning that, although the conservation of energy is not used to determine the control parameters, it is naturally satisfied along with other conservation laws. This stability analysis is inspired by [Pimenta et al. \(2013\)](#) and [Hsieh and Kumar \(2006\)](#). Our problem here can be considered as a special case of [Pimenta et al. \(2013\)](#), in which an extra term was included in the Lyapunov function as a performance measurement that characterizes the discrepancy between the resultant swarm formation and the desired shape. Another minor difference is that, in this work, the artificial viscosity term in (17) is slightly different from [Pimenta et al. \(2013\)](#) for better accuracy under low flow velocity conditions.

It can be shown that the time derivative of the Lyapunov candidate function is

$$\dot{V} = -\varepsilon \sum_i \vec{v}_i^T \vec{v}_i + \sum_i \sum_j m \frac{\mu}{\rho_i \rho_j} \frac{\vec{v}_{ij}}{\|\vec{r}_{ij}\|} \frac{dW_{ij}}{d\|\vec{r}_{ij}\|} \leq 0, \quad (21)$$

where $W_{ij} = W(\vec{r}_{ij}, h)$. Based on LaSalle's invariance theorem, the system equilibrium states $(\rho_i = \rho_0, \vec{v}_i = 0) \forall i = 1, \dots, N$ are asymptotically stable. Interested readers are referred to [Pimenta et al. \(2013\)](#) for more details.

3.3. Dimensional analysis

The proposed multi-vehicle cooperative control leads to vehicle movements that possess physical interpretations and analogies. To gain insight into these properties, it is advantageous to non-dimensionalize the control system equations. This non-dimensionalization procedure simplifies the control dynamics and discovers important independent parameters characterizing different fluid regimes. By choosing the characteristic variables and parameters ρ_0 , V_0 , c_0 , L , and μ , we obtain the following non-dimensionalized variables and parameters

$$\begin{aligned} m^* &= \frac{m}{L^d \rho_0}, & \rho^* &= \rho / \rho_0, & \vec{v}^* &= \vec{v} / V_0, \\ \vec{x}^* &= \vec{x} / L, & h^* &= h / L, & t^* &= \frac{t}{L / V_0}, \\ W^* &= L^d W, & \vec{\Pi}^* &= \frac{\vec{\Pi}}{V_0 \mu / \rho_0^2}, & c^* &= c / c_0. \end{aligned}$$

Substituting them into (4) yields the non-dimensionalized density

$$\rho_i^* = \sum_j m_j^* W_{ij}^*, \quad (22)$$

and the non-dimensional momentum equation

$$\frac{D\vec{v}_i^*}{Dt^*} = -\frac{1}{M^2} \sum_j m_j^* \left(\frac{P_i^*}{\rho_i^{*2}} + \frac{P_j^*}{\rho_j^{*2}} \right) \frac{\partial W_{ij}^*}{\partial \vec{x}_i^*} - \frac{1}{Re} \sum_j m_j^* \frac{\vec{\Pi}_{ij}^*}{r_{ij}^{*2}} \frac{\partial W_{ij}^*}{\partial r_{ij}^*}, \quad (23)$$

where the non-dimensional viscous stress is

$$\vec{\Pi}_{ij}^* = \frac{2}{\rho_i^* \rho_j^*} (\vec{v}_j^* - \vec{v}_i^*). \quad (24)$$

The non-dimensional pressure can be found as

$$P_i^* = c^{*2} \rho_i^* (\rho_i^* - 1). \quad (25)$$

This non-dimensionalization reveals two independent parameters in the momentum equation: Reynolds number Re and Mach number M . In a cooperative control problem, it is natural to define a maximal vehicle velocity and a desired inter-vehicle spacing for collision avoidance. These choices provide parameters V_0 and L in the non-dimensionalized control system equations. This leaves the choice of parameters h_i , m_i , ρ_0 , μ , Re , and M in the SPH equations. The Mach number M should be chosen to reflect the desired amount of compressibility in practice, with $M < 0.1$ being largely incompressible, but also allowing less vehicle interactions and limiting the effectiveness of the velocity consensus term. This can be done through adjusting c since the maximum vehicle speed is usually known in practice.

The relative importance of the pressure forces and the viscous forces is given by the ratio $\Phi = Re/M^2$. The choice of this ratio affects the control behavior in the same way that fluid flows at different Reynolds numbers behave differently. A low Φ results in rapid velocity diffusion between vehicles and a swarm with relatively uniform velocities, which creates a very stable swarm with slow deformation. On the other hand, high Φ causes vehicles to experience primarily pressure forces between each other with little velocity diffusion. The resulting swarm is much less cohesive, but is able to deform much more readily, which may become advantageous in domains crowded by obstacles.

4. Optimal trajectory generation

Before guiding the agents along an optimal trajectory, we first define and approximately solve the relevant fuel optimization problem. Since our focus in the present study is not on the development of new optimization routines, we apply established techniques (Latombe, 1991; LaValle, 2006) to approximate a single optimal trajectory, and then concentrate on the effectiveness of guiding a flock of vehicles along this trajectory. It is assumed that overcoming the drag force is the dominant energy cost for vehicle actuation. We attempt to minimize the total energy required to travel from an initial location \vec{x}_0 to a final destination \vec{x}_f . Denoting the agent's velocity \vec{x} and the background flow velocity $\vec{U}(\vec{x}, t)$, the normalized power usage is given by

$$P(t) = \frac{\|\dot{\vec{x}} - \vec{U}\|_2^3}{v_{\max}^3}, \quad (26)$$

and the total normalized energy, or equivalently, fuel cost can be calculated through

$$E = \frac{v_{\max}}{\|\vec{x}_f - \vec{x}_0\|} \int_{t_0}^{t_f} P(t) dt. \quad (27)$$

Here, P and E are both dimensionless and have been normalized to eliminate the inclusion of unknown drag coefficients. A value of $P(t) = 1$ corresponds to the maximum power usage, and $E = 1$ is equivalent to the energy required to move the vehicle along a straight line from \vec{x}_0 to \vec{x}_f at a speed of v_{\max} with $\vec{U} = 0$. The optimization problem is to find

$$\arg \min_{t_0, t_f, \vec{x}(t)} E, \quad (28)$$

subject to the boundary conditions

$$\vec{x}(t_0) = \vec{x}_0, \quad \vec{x}(t_f) = \vec{x}_f,$$

and constraints

$$\|\dot{\vec{x}}\| \leq v_{\max}, \quad t_{\min} \leq t_0 < t_f \leq t_{\max}.$$

Many existing techniques are available to solve this optimization problem. Again, with the optimization procedure not being a focus of this paper, existing tools are adopted to generate an energy optimal trajectory in the background flow field. The optimization problem is solved using OPTRAGEN (Bhattacharya, 2006), SNOPT (Gill et al., 2005), and FMINCON toolboxes. Given a background flow velocity field, which may be OGCM prediction outputs in practice, OPTRAGEN parameterizes the trajectory using splines and translates the minimization problem to a nonlinear programming problem that may be solved by SNOPT. Although this method is quite sensitive to the initial guess and the selected spline parameters, it generates sufficiently accurate solutions for our purposes.

Once an optimal trajectory $\vec{x}^*(t)$ has been found, a flock of vehicles can be guided along this trajectory using the flock guidance scheme discussed above. A virtual attracting particle is imagined to be navigating along the truly optimal trajectory and the flock of agents follows closely along due to the resulting attracting forces. As long as the flock radius is properly chosen such that the background flow velocity variation across the flock is small, and the flock remains close to the attracting particle, the proposed control scheme results in nearly optimal trajectories for each agent.

Theorem 1. For a non-rotating, rigid flock² following the optimal trajectory $\vec{x}^*(t)$, the total actuation energy for each flock agent is close to the optimal energy associated with $\vec{x}^*(t)$ if $\max(\|\vec{J}\|) \cdot \|\vec{\delta x}\| \ll 1$, with $\max(\|\vec{J}\|)$ being the maximum background flow velocity gradient on the path and $\|\vec{\delta x}\|$ being a bound on the flock radius.

Proof. Given an agent in this rigid flock that follows a trajectory $\vec{x}(t) = \vec{x}^*(t) + \vec{\delta x}$, where $\vec{\delta x}$ is the relative position vector of the agent with respect to the virtual attractor, a Taylor series expansion gives the background velocity experienced by this agent as

$$\vec{U}(\vec{x}(t), t) = \vec{U}(\vec{x}^*(t), t) + \vec{J}(\vec{\xi}, t) \vec{\delta x}, \quad (29)$$

where \vec{J} is the Jacobian of the background velocity field and $\vec{\xi}$ is a point between \vec{x} and \vec{x}^* . The power usage is then given by

$$P(t) = \frac{\|\dot{\vec{x}} - (\vec{U}(\vec{x}^*(t), t) + \vec{J}(\vec{\xi}, t) \vec{\delta x})\|_2^3}{v_{\max}^3}. \quad (30)$$

Let

$$P^*(t) = \frac{\|\dot{\vec{x}}^* - \vec{U}(\vec{x}^*(t), t)\|_2^3}{v_{\max}^3} = \frac{\|\dot{\vec{x}} - \vec{U}(\vec{x}^*(t), t)\|_2^3}{v_{\max}^3} \quad (31)$$

be the power usage of the optimal trajectory, then the actual power usage of an agent in the rigid flock can be evaluated as

² This condition will lead to a loose upper bound of the total actuation energy of each flock agent. When the flock is allowed to rotate and deform, the total actuation energy of each flock agent will be even closer to the optimal energy.

$$\begin{aligned}
 P(t) &\leq \left(\frac{\|\vec{x} - \vec{U}(\vec{x}^*, t)\|}{v_{\max}} + \frac{\|\vec{J}(\vec{\xi}, t)\| \cdot \|\vec{\delta x}\|}{v_{\max}} \right)^3 \\
 &\leq \left(P^*(t)^{1/3} + \frac{\|\vec{J}\| \cdot \|\vec{\delta x}\|}{v_{\max}} \right)^3 \\
 &\leq P^*(t) + 3P^*(t)^{2/3} \frac{\|\vec{J}\| \cdot \|\vec{\delta x}\|}{v_{\max}} + 3P^*(t)^{1/3} \left(\frac{\|\vec{J}\| \cdot \|\vec{\delta x}\|}{v_{\max}} \right)^2 \\
 &\quad + \left(\frac{\|\vec{J}\| \cdot \|\vec{\delta x}\|}{v_{\max}} \right)^3.
 \end{aligned} \tag{32}$$

Given this upper bound on the power usage, the total energy used is bounded by

$$\begin{aligned}
 E &\leq E^* + 3 \frac{\max(\|\vec{J}\|) \cdot \|\vec{\delta x}\|}{\|\vec{x}_f - \vec{x}_0\|} \int_{t_0}^{t_f} P^*(t)^{2/3} dt \\
 &\quad + 3 \frac{\left(\max(\|\vec{J}\|) \cdot \|\vec{\delta x}\| \right)^2}{v_{\max} \|\vec{x}_f - \vec{x}_0\|} \int_{t_0}^{t_f} P^*(t)^{1/3} dt \\
 &\quad + \frac{\left(\max(\|\vec{J}\|) \cdot \|\vec{\delta x}\| \right)^3}{v_{\max}^2 \|\vec{x}_f - \vec{x}_0\|} (t_f - t_0),
 \end{aligned} \tag{33}$$

where E^* is the total actuation energy consumption for the optimal trajectory. For a given flow region, (33) provides an upper bound for the actuation energy cost of each agent. \square

Given $\max(\|\vec{J}\|)$ known beforehand, the flock size and the neutral density can be properly chosen such that $\max(\|\vec{J}\|) \cdot \|\vec{\delta x}\| \ll 1$ and the energy cost has a tighter bound close to the optimal energy cost. As indicated by all the testing results we will be showing in Section 5, real actuation cost, when the flock is allowed to rotate and deform, can be expected to be further closer to the optimal energy cost. Note that the integrals in (33) are determined solely based on the optimal trajectory, and $\|\vec{J}\|$ is dependent on the properties of the background flow field. The energy bound is equal to the optimal trajectory energy usage plus three additional terms involving $\|\vec{J}\| \cdot \|\vec{\delta x}\|$. Since $\|\vec{J}\|$ represents the gradient of the background velocity field and $\|\vec{\delta x}\|$ is bounded by the maximum flock radius, *the trajectories are nearly-optimal for velocity fields with spatial gradients that are small on the scale of the swarm size*. In other words, vehicle trajectories are guaranteed to be nearly fuel optimal if $\|\vec{J}\| \cdot \|\vec{\delta x}\| \ll 1$. Additionally, we expect the energy cost per agent to scale as

$$E \approx E^* + c_1 R + c_2 R^2 + c_3 R^3, \tag{34}$$

where R is the radius of the flock that is dependent on the number of agents through $R \propto \sqrt{N}$, and c_1 , c_2 , and c_3 are constants.

5. Simulation results in ocean flows

To demonstrate the feasibility of the proposed multi-vehicle cooperative control and flock guidance scheme, we investigate tests in two artificial flow fields that resemble common features observed in real-world ocean flows: a time-dependent double-gyre (Shadden et al., 2005) and a meandering jet (Samelson, 1992), as well as a practical background flow field in the Gulf of Mexico reconstructed based on ocean current model data. We consider two-dimensional vehicle kinematics, $\dot{r}_i = v_i^{\text{rel}} + V_i^{\text{flow}}$, where v_i^{rel} represents the velocity of vehicle i with respect to the background flow, and V_i^{flow} represents the background flow velocity at the location of vehicle i . Constraints on v_i^{rel} are introduced in all following simulations such that the resulting surge

speed and turning rate do not exceed the actuation limits of a nonholonomic vehicle. Neglecting the vehicle dynamics is approximately valid when the dominant flow scales are much larger than the vehicle size, as is true for our problem of interest. Constraints on the maximum vehicle velocity with respect to the background flow and the minimum turning radius are considered. All vehicles are assumed to have localization capabilities and be able to perform two-way communication in a confined range. The effects of localization errors caused by acoustic communication is beyond the scope of this paper.

All three tests are performed in simulation, and flock sizes ranging from $N = 1$ to $N = 500$ are considered. Based on the simulation results with different numbers of vehicles, we analyze the scaling of the average energy consumption per vehicle versus the flock size. This scaling enables the predictability of the per-vehicle energy consumption that one can expect when the proposed algorithm is applied to potential applications with larger numbers of agents compared with conventional underwater vehicle applications. These simulations were performed with an SPH force ratio of $\phi = 5$ (as discussed in Section 3), a smoothing width $h = 500$ m for the vehicles, and a smoothing width for the virtual attractor approximately equal to the flock radius.

5.1. Double-gyre flow

The double-gyre phenomena in large-scale ocean circulation is typical of the northern mid-latitude ocean basins. It is quite dominant and persistent in oceans and consists of a sub-polar and a sub-tropical gyres. The time-dependent double-gyre is an oscillating perturbation to two counter-rotating gyres. As a major type of ocean circulations, several main features of the double-gyre phenomena have been identified through analyzing the observational data and numerical simulations (Jiang et al., 1995; Speich and Ghil, 1994; Speich et al., 1995). A simplified double-gyre model has been used extensively in many cases (Shadden et al., 2005). A snapshot of the velocity field is shown in Fig. 4.

The velocity field for this flow is defined by the stream function

$$\psi(x, y, t) = A \sin(\pi f(x, t)) \sin(\pi y), \tag{35}$$

where the time-dependent parameters are

$$\begin{aligned}
 f(x, t) &= a(t)x^2 + b(t)x, \\
 a(t) &= \epsilon \sin(\omega t), \\
 b(t) &= 1 - 2\epsilon \sin(\omega t).
 \end{aligned} \tag{36}$$

The velocity field can be calculated through

$$u = -\frac{\partial \psi}{\partial y}, \quad v = \frac{\partial \psi}{\partial x}. \tag{37}$$

This velocity field is defined on the non-dimensional domain $[0, 2] \times [0, 1]$. To provide a more realistic scenario, the domain was rescaled to 200 km \times 100 km by simply evaluating $(u, v) = (u(x/L, y/L, t), v(x/L, y/L, t))$, where the length-scale was chosen as $L = 100$ km. For reference, the Red Sea is approximately 200 km wide. The flow parameters were selected such that the maximum flow

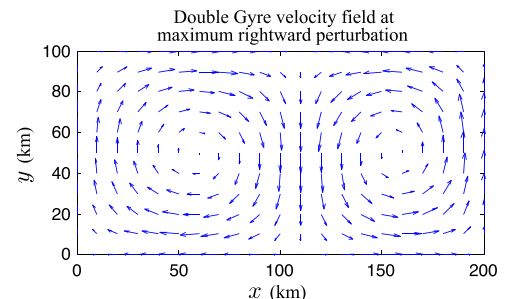


Fig. 4. The double-gyre velocity field at time $t = T/4$, maximum eastward (rightward) perturbation, where T is the period of oscillation.

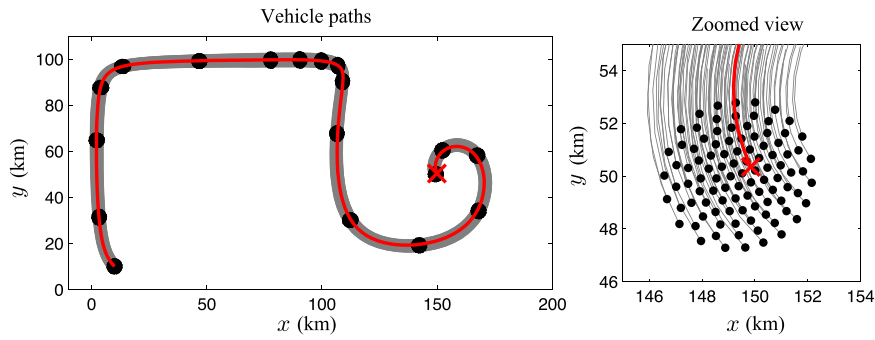


Fig. 5. An example of the nearly optimal vehicle trajectories in the double-gyre flow. The left figure plots the trajectories of a flock of 100 vehicles. Vehicle trajectories are plotted as gray curves, vehicle positions are shown as black dots every 12 h, the optimal trajectory is shown as a red curve, and the final goal location is a red x. The trajectories begin at the bottom left and end at (150, 50). The zoomed figure at right shows the flock structure at the final location. (For interpretation of the references to color in this figure legend, the reader is referred to the web version of this article.)

speed is 1 m/s ($A = 1/\pi$), the maximum perturbation of the flow is approximately 10 km ($\varepsilon = 0.1$), and the period of the time-dependent oscillation is roughly 87 h ($\Omega = 2 \times 10^{-5}$).

The optimal trajectory begins at $\vec{x}_0 = (10 \text{ km}, 10 \text{ km})$ and traverses the domain to reach the final destination $\vec{x}_f = (150 \text{ km}, 50 \text{ km})$. It was calculated as discussed in Section 4. The maximum forward speed and the minimum turning radius of the vehicles are limited to realistic values of 0.3 m/s and 1 m, respectively. The minimum distance between any two vehicles in any of the swarms tested here was 104 m, approximately 1/5 of the smoothing length. Fig. 5 shows an overview of one set of nearly optimal trajectories. Trajectories of 100 vehicles are shown in gray, along with their positions every 12 h (black dots), the optimal trajectory (red curve), and the final destination (red x). A zoomed view of the final vehicle positions is shown such that the structure of the flock can be visualized. The vehicles closely follow the optimal trajectory with the flock rotating and deforming slightly under the influence of the background flow. Swarms of other sizes exhibit similar behavior.

The normalized energy cost for the agents in each flock is plotted in Fig. 6. Flocks of 1, 3, 5, 7, 10, 15, 20, 30, 50, 75, 100, 150, 200, 300, and 500 vehicles were investigated. The maximum, minimum, and mean normalized actuation energy costs versus the flock radius are shown. These energy costs are expected to scale according to (34) so a least squares best fit is performed for the maximum and mean energy costs for the flocks of 10, 20, 50 and 100 vehicles, and plotted in the same figure. These flocks have radii ranging from about 340 m to 1.35 km. This fit allows us to predict the fuel costs of larger flocks based on the radius and results in errors of less than 1% for flocks of up to 150 agents. For larger flocks, the fitting error grows as does the energy cost. This is expected since the velocity gradients in this flow are $\max(\|\nabla \vec{v}\|) \approx 4 \times 10^{-5} \text{ s}^{-1}$. So for these larger flocks, $\|\nabla \vec{v}\| R > 0.15 \text{ m/s}$, and the trajectories far from the flock center are no longer expected to be nearly optimal.

Additionally, the fitting error is due to over-estimation of actuation

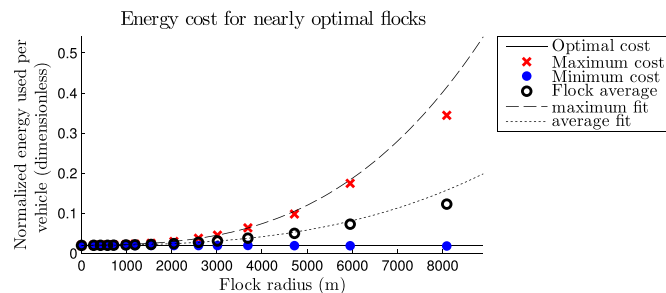


Fig. 6. The energy cost for flocks of size 1, 3, 5, 7, 10, 15, 20, 30, 50, 75, 100, 150, 200, 300, and 500 along with best-fit curves for the maximum and mean cost. The best-fit curves are based only on flocks of 10, 20, 50, and 100 agents, but provide good results when extrapolating to 150 vehicles.

energy costs. This can be explained given the fact that the flock is free to rotate as it moves with the flow, which was not considered in the analysis in Section 4. The rotation is caused by the influence of the background flow. It decreases the velocity difference between the agents and the background flow, reducing the true actuation energy cost. This effect is more pronounced in larger flocks since the effective torque on the agents is proportional to the flock radius.

5.2. Meandering jet

The meandering jet velocity field was introduced by Samelson (1992) and was intended to be similar to jets that can appear in ocean flows. It consists of a sinusoidal jet of higher velocity fluid through an otherwise quiescent domain. The stream function for the flow is given by

$$\psi = \psi_0 \left[1 - \tanh \left(\frac{y - A \cos(k(x - ct))}{\lambda \sqrt{1 + k^2 A^2 \sin^2(k(x - ct))}} \right) \right], \quad (38)$$

and parameters $A = 1$, $K = 0.5$, $c = 0.5$, $\lambda = 1.5$, and $\psi_0 = 5.4$ were used. This creates a maximum flow speed of 3.6 m/s. Similar to the double-gyre flow field, the domain was scaled by a factor of 10,000 for a more realistic size, resulting in a jet width of approximately 40 km. The optimal trajectory begins at $\vec{x}_0 = (0 \text{ km}, -60 \text{ km})$ and ends at $\vec{x}_f = (150 \text{ km}, 60 \text{ km})$. A maximum vehicle speed of 1.2 m/s was used. A plot of the meandering jet flow and the trajectories of a 100-agent flock are shown in Fig. 7.

Simulations were performed with the same flock sizes as used in the double-gyre flow up to 300 agents, and the resulting actuation energy costs are shown in Fig. 8 for flocks of up to 100 agents. Again, least squares best fits were performed on the data for maximum and mean energy costs. The fits considered only flocks of size 10, 20, 50, and 100 and the fitting results are also presented in Fig. 8. For all flocks of less than 100 agents, error in the curves is less than 0.4%, providing a good prediction of the energy costs for these flock sizes.

In the meandering jet, larger flocks of 150, 200, and 300 agents were also tested. In this flow field, $\max(\|\nabla \vec{v}\|) \approx 1.9 \times 10^{-5} \text{ s}^{-1}$ such that $\|\nabla \vec{v}\| R > 0.07, 0.09, 0.11$ for the flocks of 150, 200, and 300 agents with R being flock radii. This does not satisfy the condition that flow velocity spatial variation across the flock is small. As a result, actual vehicle paths are no longer nearly fuel-optimal. In fact, the jet flow is strong enough such that some of the agents in the 200 and 300 agent flocks become separated from the flock while traversing the jet and are not able to rejoin the flock. This can be addressed by increasing the neutral density such that the flock radius decreases.

It is worth mentioning that the SPH-based flock control scheme is a fully distributed method that only requires local information within the sensor range. In practice, the smoothing kernel can be chosen to be compactly supported within the sensor range. Therefore, inter-agent

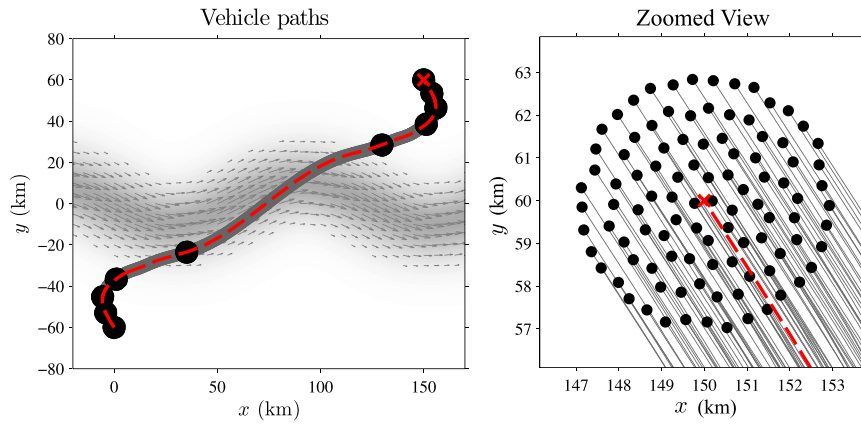


Fig. 7. The meandering jet velocity field with the optimal trajectory plotted in red, the agent paths in gray, and 10 of the flock positions in black. This flock consists of 100 agents and moves from bottom left to top right. A zoomed view of the flock configuration at the goal location is shown at right. (For interpretation of the references to color in this figure legend, the reader is referred to the web version of this article.)

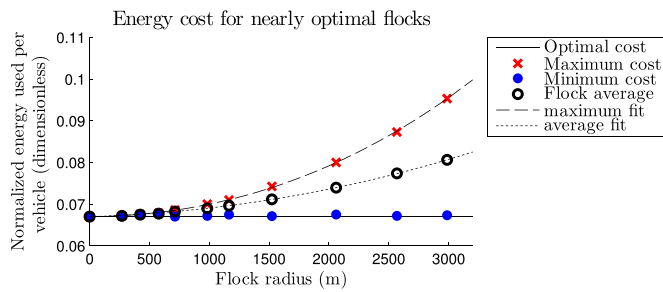


Fig. 8. Energy cost for flocks to traverse the meandering jet domain. The maximum energy cost for the last two flocks is off the scale. The dotted and dashed lines are fits to the mean and maximum energy cost in the flocks. The best fit curves are based on only the 10, 20, 50, and 100 agent flocks and provide excellent prediction for up this range.

communication can be achieved in a single-hop manner. In the context of multi-vehicle cooperation where inter-vehicle communication is originally required, the proposed flock guidance method does not require further vehicle capabilities or generate extra communication costs. For a homogeneous fleet, of which agents have the same virtual mass and motion constraints, information transmitted through communication only includes local virtual density, pressure, location, and velocity. Moreover, communication frequency required for reasonably good flock performance is usually very low. For instance, in the case with the double-gyre flow field, the reported performance was achieved with communication interval of approximately 0.7 h.

5.3. Ocean current model

In order to further demonstrate the robustness of the proposed flock control and guidance scheme, simulation tests in a reconstructed ocean flow field were performed. In this study, we use hourly surface current model data provided by HYCOM Gulf of Mexico (Cummings and Smedstad, 2013). The Gulf of Mexico nowcast/forecast system has $1/25^\circ$ (≈ 3.5 km) equatorial resolution and $1/25^\circ \times \cos(\text{latitude})$ latitudinal resolution (Naval Research Laboratory, 2015). Fig. 9(Left) shows linearly-interpolated surface current velocity at 9 p.m. on June 10th, 2015. The maximum flow speed is approximately 2.3 m/s, which is commensurate with, if does not exceed, typical underwater vehicle velocities. In this simulation, we consider the more severe case where vehicles' maximum flow-relative velocities are mostly smaller than typical ocean currents.

We selected the surface current data of the duration from 2015-06-01 00:00:00 to 2015-06-14 00:00:00. In order to reconstruct the background flow field using the ocean current data set with higher accuracy, we interpolated the background flow field in both space and time using tensor product B-splines. The general B-spline param-

eterizes the eastward velocity $u(\text{lon}, \text{lat}, t)$ and the northward velocity $v(\text{lon}, \text{lat}, t)$ as

$$u(\text{lon}, \text{lat}, t) = \sum_{i=1}^p \sum_{j=1}^q \sum_{k=1}^r B_{i,s_{ix}}(\text{lon})B_{j,s_{iy}}(\text{lat})B_{k,s_{it}}(t)c_{1,ijk},$$

$$v(\text{lon}, \text{lat}, t) = \sum_{i=1}^p \sum_{j=1}^q \sum_{k=1}^r B_{i,s_{ix}}(\text{lon})B_{j,s_{iy}}(\text{lat})B_{k,s_{it}}(t)c_{2,ijk}, \quad (39)$$

where p , q , and r are numbers of coefficients of the corresponding B-spline functions, $c_{1,ijk}$ and $c_{2,ijk}$ are the coefficients, and s -terms are orders of splines. In this case, we focus on the domain $(89W, 86W) \times (25.5N, 27.5N)$, where drastic current changes occur. We chose the orders of splines to be 4, and let $p = 76$, $q = 57$, $r = 252$.

In this set of simulations, we apply the built-in optimal solver *fmincon* in MATLAB to generate the fuel optimal trajectory since analytical expressions of the background flow field, as required by OPTRAGEN, are not easily available. A local optimal trajectory from $(-88^\circ, 27.1^\circ)$ to $(-87.2^\circ, 25.9^\circ)$ is shown in Fig. 9(Right). The duration of the operation is about 10.5 days.

Simulations were performed with the same flock sizes as used previously up to 500 agents. Major parameters used in this set of simulations are: the maximum vehicle velocity relative to the ambient water $v_{\text{max}} = 0.3$ m/s; the minimum turning radius $R_{\text{min}} = 1$ m; neutral density $\rho_o = 1$ kg/m; artificial drag coefficient $e = 0.05 \text{ s}^{-1}$; the smoothing length $h = 500$ m; SPH force ratio $\phi = 5$; control frequency $f = 0.1$ Hz. In the selected domain, the maximum current velocities are 2.27 m/s in the eastward direction and 2.48 m/s in the northward direction. These velocities are almost an order of magnitude higher than the maximum vehicle flow-relative velocity. Fig. 10 shows the trajectories of 100 vehicles.

The normalized energy cost for the agents in each flock is presented in Fig. 11. Flocks of 1, 3, 5, 7, 10, 15, 20, 30, 50, 75, 100, 125, 200, 300, and 500 vehicles were investigated. The maximum, minimum, and mean normalized actuation energy costs versus the flock radius are shown. The least squares best fits were performed on the data for maximum and mean energy costs of flocks with sizes of 10, 20, 50, and 100.

For all flocks of less than 150 vehicles, energy costs scale according to (34), and the fitting error is less than 1%. For larger flock sizes, however, the fitting error grows along with the energy cost, especially for average cost fitting. The radii of the flocks range from approximately 4.7 km to about 8.1 km for flocks of size 200, 300, and 500. In fact, in this flow field, $\max(\|\nabla \vec{v}\|) \approx 2.1188 \times 10^{-5} \text{ s}^{-1}$ along the optimal trajectory such that, for these large flocks, $\|\nabla \vec{v}\| R$ is larger than 0.1, 0.13, and 0.17, respectively. The condition for vehicle energy cost to be nearly optimal, $\|\nabla \vec{v}\| R \ll 1$, ceased to be satisfied. In practice, this can be remedied through properly increasing the reference density

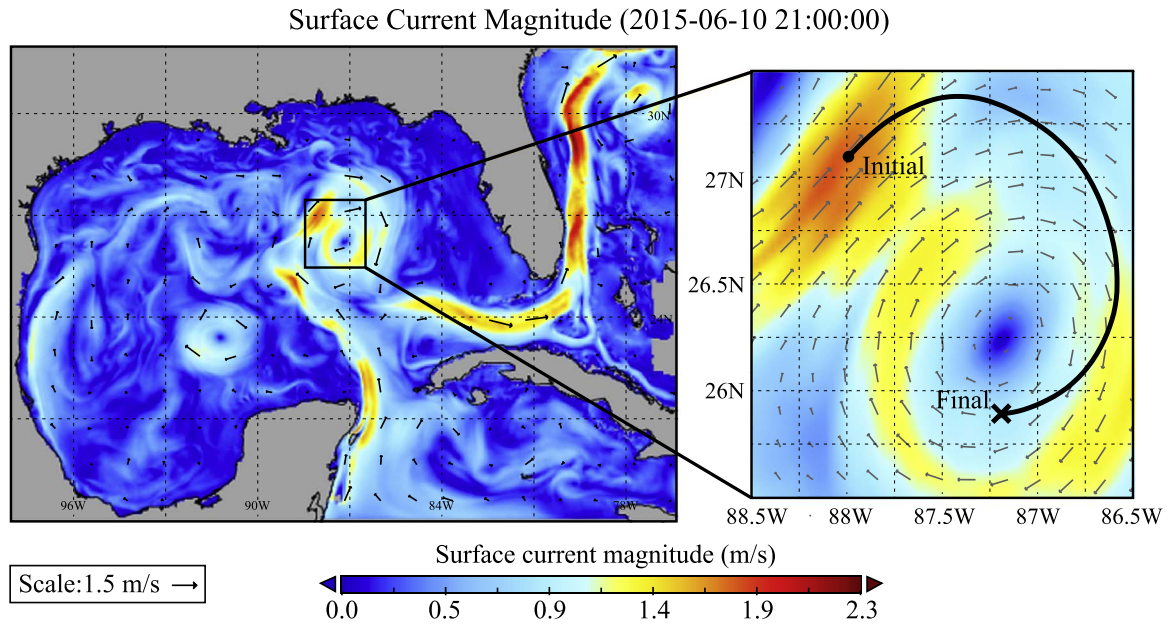


Fig. 9. Surface current velocity of Gulf of Mexico at 21:00:00 on June 10, 2015 (Left) based on data sets generated by HYCOM Gulf of Mexico. A local, fuel-optimal trajectory is shown on the zoomed figure (Right) from the initial location (− 88°, 27.1°) to the final location (− 87.2°, 25.9°).

p_0 or decreasing the smoothing length h in order to decrease the resultant flock radii.

Remark 1. (Energy optimality): Our focus in this paper is on the optimization of vehicles’ actuation energy costs. Since vehicles navigate along trajectories similar to the energy-optimal trajectory, the difference in energy costs between an actual vehicle and the virtual attractor mainly results from the differences in background flow velocities along respective trajectories. As long as vehicles are close to the optimal trajectory such that the velocity gradients in the flow field are small, then their actuation energy costs are close to optimal. This is because the only additional cost is to overcome the velocity difference between the background flow at their location and the flow along the optimal trajectory.

Remark 2. (Inter-vehicle spacing): The average inter-vehicle spacing is problem-dependent, and easily adjustable through changing the smoothing length h and the virtual mass m , based on the situation. In a spatiotemporally changing flow field, the energy optimality of a vehicle depends on its distance from the virtual attractor, and the differences in background flow velocities experienced by the vehicle and the virtual attractor. Therefore, smaller flock radii, hence small inter-vehicle spacings, are desirable in highly turbulent background flows with

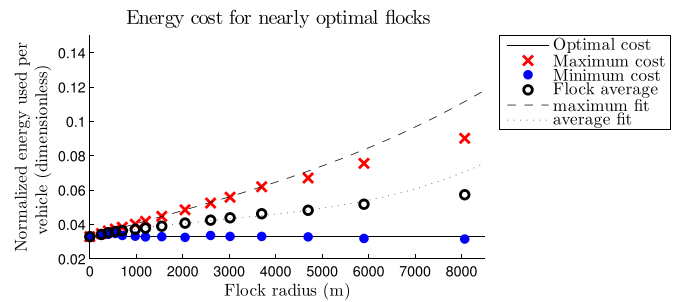


Fig. 11. Energy cost for flocks traveling in ocean flows reconstructed based on HYCOM Gulf of Mexico surface current velocity data. The normalized energy cost for agent flocks of size 1, 3, 5, 7, 10, 15, 20, 30, 50, 75, 100, 125, 200, 300, and 500 are shown along with best-fit curves for the maximum and mean cost.

large spatial variations in flow velocities. Although smaller spacings are always desirable from an energy optimality perspective, some minimum spacing is required to provide a safety margin and avoid inter-vehicle collisions.

Remark 3. (Implementation considerations): The proposed multi-vehicle flocking and guidance scheme aims at generating local control

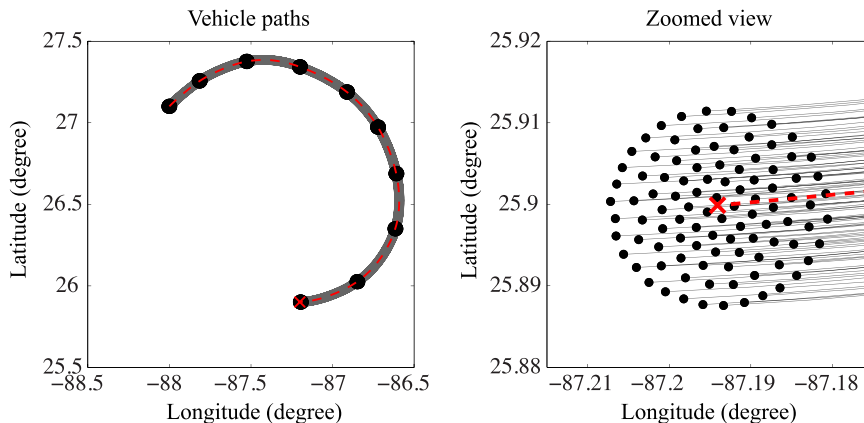


Fig. 10. Paths of 100 vehicles (solid gray) tracking the local, fuel-optimal trajectory (dash red) in an ocean flow field along with 10 flock positions (black). A zoomed view of the flock configuration approaching the goal location is shown at right. (For interpretation of the references to color in this figure legend, the reader is referred to the web version of this article.)

polices in the forms of virtual interaction forces among vehicles, without imposing any requirements in their implementations or any specifications in vehicle dynamics. In all reported simulations, holonomic vehicle kinematics were used with motion constraints on the minimum turning radius and the maximum forward velocity relative to the surrounding fluid to mimic a nonholonomic vehicle. Therefore, our approach is readily applicable to most underwater vehicle platforms including holonomic remotely operated vehicles (ROVs) or nonholonomic AUVs with control surfaces. In long-duration operations, underwater gliders are suitable alternatives to AUVs. The proposed multi-vehicle control and guidance method can be applied as well with minimum modifications to address their periodic, vertical movements. However, similar to most vehicle control algorithms, one should expect the best performance in applications with holonomic underwater vehicles.

Remark 4. (Scalability): Our proposed approach is fully distributed owing to the selection of kernel functions with compact support. The computational complexity per vehicle is independent of the total number of agents, and scales linearly as $\mathcal{O}(N_a + 1)$, with N_a representing the number of adjacent vehicles in the region defined by the smoothing kernel function, and the “1” representing the computation regarding to the virtual attractor. Since the optimal trajectory only needs to be computed for the virtual attractor in an offline fashion, the associated computational time is entirely independent of the number of agents. In the case where the kernel distance is smaller than the communication range, it is also necessary to filter out vehicles that are in the communication range, but not within the kernel distance. The overall computational complexity becomes $\mathcal{O}(N_c + 1)$, where N_c denotes the number of neighboring vehicles in the communication range and $N_c \geq N_a$.

Remark 5. (Communication constraints): Implementing a cooperative control approach to an AUV swarm requires careful deliberation in addressing the complication due to unreliable acoustic communication channels, including the constraints on communication range, network topology, bandwidth, and latency. In this regard, when implementing the proposed cooperative control approach, the smoothing length should be properly selected to reflect the limitation on communication range. The number of neighbors each vehicle is allowed to interact with can be adjusted implicitly by the reference density p_0 . For the inter-vehicle separation and vehicle velocities relevant to our application, the effect of communication delay on vehicles’ energy consumption or flocking performance is considered negligible. Rigorously addressing these communication constraints on a theoretical level will be the topic of a future publication. Several existing studies have tackled these issues to some extent for similar applications including multi-agent target tracking (Sabatini et al., 2014), formation control (Fax and Murray, 2004), and consensus (Olfati-Saber and Murray, 2004; Moreau, 2005). Interested readers are also referred to Shaw and Mohseni (2011) for a performance evaluation of the SPH-based cooperative control method in an aerial vehicle implementation in the presence of communication range limitation, packet loss, and transmission error.

6. Importance of velocity consensus in multi-agent flocking

The SPH-based multi-vehicle control scheme not only addresses swarming and collision avoidance gracefully, the inherent swarm viscosity plays an essential role in the flocking performance. In addition, our physical intuition enables us to better understand and control the velocity consensus effect in flocking. In this section, we show the importance of the velocity matching effect introduced by fluid viscosity in flocking performance. To do so, we compare the flocking performance of the fluid-based control scheme and a generic artificial potential based control scheme, which only focuses on maintaining proper inter-agent spacings, in terms of collision avoidance efficacy and

actuation energy consumption. We will show that the presence of swarm viscosity results in more consistent inter-vehicle spacings and lower energy usage in all the tested cases.

6.1. Generic artificial potential based multi-vehicle control scheme

The artificial potential based multi-vehicle control method originates from the physics-inspired techniques using potential fields (Khatib, 1986). It has been widely adopted to achieve multi-vehicle swarming and collision avoidance by mimicking the interactions among adjacent molecules or atoms (Hsieh and Kumar, 2006; Leonard and Fiorelli, 2001; Spears et al., 2005). The interested reader is referred to Spears and Spears (2012) and the references therein for more details about this approach. Under this multi-vehicle control scheme, each vehicle is associated with a potential field, such as the Lennard-Jones potential or the gravitational potential, and the inter-vehicle forces are determined by the gradient of the total potential. To properly demonstrate the importance of the swarm viscosity effect in the fluid-based control scheme, the potential function was designed such that non-moving, two-particle systems (i.e. two interacting vehicles or a vehicle and a reduced density attractor) experience identical forces under both control schemes.

Recall that the non-dimensional SPH formulation was discussed in Section 3.3. Accordingly, a non-dimensional artificial potential control scheme can be formulated. We assume unit mass for vehicle particles such that the acceleration is given by

$$\frac{d\vec{v}_i}{dt} = -\frac{1}{m_i} \sum_j \nabla_i \phi_j, \quad (40)$$

where ϕ is the artificial potential function to be decided. The potential function ϕ is commonly designed such that vehicle i experiences a repulsive force as it approaches neighboring vehicle j and an attractive force as it moves away. For a direct comparison between these two control schemes, the potential function is designed based on the smoothing kernel function (1) so it has the form

$$\phi_j = \kappa_j h_j \begin{cases} 1 - \frac{3}{2}s^2 + \frac{3}{4}s^3 & \text{if } 0 \leq s \leq 1 \\ \frac{1}{4}(2-s)^3 & \text{if } 1 < s \leq 2 \\ 0 & \text{if } s > 2 \end{cases}, \quad (41)$$

where s is defined in the same way as in (1) such that the potential function has the same profile as the proposed fluid-based method. The gradient of this potential function is

$$\nabla_i \phi_j = \kappa_j \begin{cases} -3s + \frac{9}{4}s^2 & \text{if } 0 \leq s \leq 1 \\ -\frac{3}{4}(2-s)^2 & \text{if } 1 < s \leq 2 \\ 0 & \text{if } s > 2 \end{cases}, \quad (42)$$

the magnitude of which is proportional to the constant κ_j . It should be noticed that κ is not a normalization constant here. Instead, it controls the strength of the potential and may take either positive or negative values.

The artificial potential based control scheme can be non-dimensionalized using the dimensionless variables and parameters as follows

$$m^* = m/m_0, \quad \kappa^* = \frac{L}{m_0 V_0^2} \kappa, \quad \vec{x}^* = \vec{x}/L, \\ h^* = h/L, \quad \vec{v}^* = \vec{v}/V_0, \quad t^* = \frac{t}{L/V_0}, \quad \phi^* = \frac{\phi}{m_0 V_0^2}.$$

This leads to the dimensionless system dynamics given by

$$\frac{d\vec{v}_i^*}{dt^*} = -\frac{1}{m_i^*} \sum_j \nabla_i^* \phi_j^*, \quad (43)$$

$$\phi_j^* = \kappa_j^* h_j^* \begin{cases} 1 - \frac{3}{2}s^2 + \frac{3}{4}s^3 & \text{if } 0 \leq s \leq 1 \\ \frac{1}{4}(2-s)^3 & \text{if } 1 < s \leq 2 \\ 0 & \text{if } s > 2 \end{cases} \quad (44)$$

It is worth mentioning that the dimensionless parameters vanish, leaving κ^* as the only independent parameter to be determined for the artificial potential scheme.

We restrict the analysis to the cases that all vehicles have the same mass m^* , kernel width $h^* = 1$, and potential strength κ^* . The virtual attracting particle has a different kernel width h_A^* and a negative potential strength $\kappa_A^* < 0$. The acceleration of a single vehicle i can be calculated as

$$\frac{d\vec{v}_l^*}{dt^*} = - \sum \frac{\kappa_l^*}{m^*} \begin{cases} -3s + \frac{9}{4}s^2 & \text{if } 0 \leq s \leq 1 \\ -\frac{3}{4}(2-s)^2 & \text{if } 1 < s \leq 2 \\ 0 & \text{if } s > 2 \end{cases} \quad (45)$$

where $l = j$ for a neighboring vehicle j , and $l = A$ for the virtual attractor. The ratio κ_l^*/m^* is the only parameter to be adjusted.

6.2. Test results

For a direct comparison, we set $m^* = 1$ and chose the parameters κ_j^* and κ_A^* such that the work required to bring two vehicles together from infinity is the same under both the artificial potential based scheme and the fluid-based scheme. The same requirement was made for the virtual attractors. This results in the relationships

$$\kappa^* = \frac{0.6136}{M^2 h_A^*}, \quad \kappa_A^* = -\frac{1}{M^2 h_A^*} \quad (46)$$

The resulting non-dimensional control forces are shown in Fig. 12 for parameters $M = 1$, $Re = \infty$ (inviscid), and $V_o = 1$. The attracting particles exert identical forces in both control schemes. The non-viscous, inter-vehicle forces for the two control schemes are qualitatively similar. The SPH force weights more heavily towards small vehicle separations. This is because the density increases as vehicles approach each other, generating larger repelling forces than the potential control scheme, where the force scaling is constant.

The most significant difference between the two control schemes is the presence of the viscous forces in the fluid-based control scheme. Recall that, in the non-dimensional SPH formulation, the viscous stress (24) results in a viscous damping force acting in opposition to the velocity difference between two vehicles. In this way, it acts as a velocity consensus term for the vehicle swarm. The effect is that, as we will show explicitly in the following simulations, low Reynolds number fluid control schemes, corresponding to relatively large viscosity, result in more coherent swarm motions compared to potential function

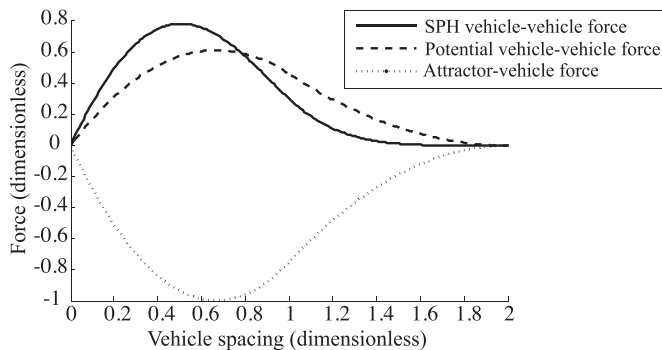


Fig. 12. The control forces for the inviscid SPH and potential control algorithms. Parameters used are $M = 1$, $Re = \infty$, and $V_o = 1$. The attractor particles exert the same force on the vehicles in both control schemes.

schemes.

To demonstrate the effect of viscous forces in the fluid-based control scheme, we present the results of multiple tests for the two algorithms in a domain without background flows. In all of the following simulations, a total number of eleven vehicles were used. These vehicles were assumed to have the minimum velocity $V_{\min} = 0.3$ m/s, the maximum velocity $V_{\max} = 1.0$ m/s, and the minimum turning radius of 5 m. A Mach number of $M = 2$ was chosen such that the swarm is compressible and a Reynolds number of $Re = 0.1$ was used, giving $\phi = 0.025$ in the SPH simulation. Two scenarios that are being considered are a stationary attractor that may represent a base station or a hot spot of an event of interest, and a moving attractor following a circular path in various speeds.

6.2.1. Stationary attractor

In the first test, a stationary attractor is fixed to the origin. The vehicles are initially placed on a hexagonal grid around the origin with inter-vehicle spacings of $1.5h$ and are given a random initial heading. Due to the minimum velocity constraint on these vehicles, no static equilibrium state is possible under either control scheme. However, after around 100 s, the SPH-based control scheme results in a coordinated swarm navigating in tight circles determined by the minimum turning radius (5 m) and maintaining a relatively stable formation (Fig. 13(Left)). Once established, this stable navigation state persists indefinitely.

The lack of velocity consensus effect in the generic potential function based control scheme results in a highly disordered system. As shown in Fig. 13(Right), the vehicle group remains disordered, exhibiting chaotic motion patterns, even after several minutes of navigation. Under this control scheme, the control forces only act to steer vehicles towards or away from each other; their motion directions are not considered. Unfortunately, the constraints on turning radius and the lack of velocity consensus effect lead to vehicle collisions in this case. In Fig. 13(Right), several of the vehicles are either very close together or are headed directly toward each other with collisions imminent.

Moreover, the lack of velocity matching has an extra effect of increasing the average vehicle speed, leading to increased fuel usage for the potential function based control scheme in this example. To quantify this effect, we assume that drag is the main force that must be overcome by the vehicles and it is proportional to the magnitude of velocity squared. Under these assumptions, the fuel usage E can be evaluated as

$$E \propto \int_{t_0}^{t_f} \|\vec{v}\|^2 dt. \quad (47)$$

Even without knowing the appropriate drag coefficients, this allows us to compute the relative fuel usage for the two control schemes. For the stationary attractor case, vehicles consume 47.5% less fuel on average under the SPH-based control scheme than the artificial potential based control scheme.

6.2.2. Circular attractor path

The second test involves guiding the vehicle group along a circular path with various attractor speeds. The radius of the circular path is set to 50 m and the tested attractor speeds vary from 0.2 m/s to 1.5 m/s. All other parameters are kept the same as the previous test. Fig. 14 shows the performance of both control schemes under different guiding speeds.

For the case where the attractor moves slower than the minimum vehicle speed, vehicles need to circle back every now and then until the attractor catches up. The SPH-based control scheme maintains relatively consistent vehicle movement across the flock while the potential function based approach leads to disorganized vehicle motions due to the lack of inter-vehicle velocity matching effect. In the opposite case, when the attractor's speed exceeds the maximum vehicle speed,

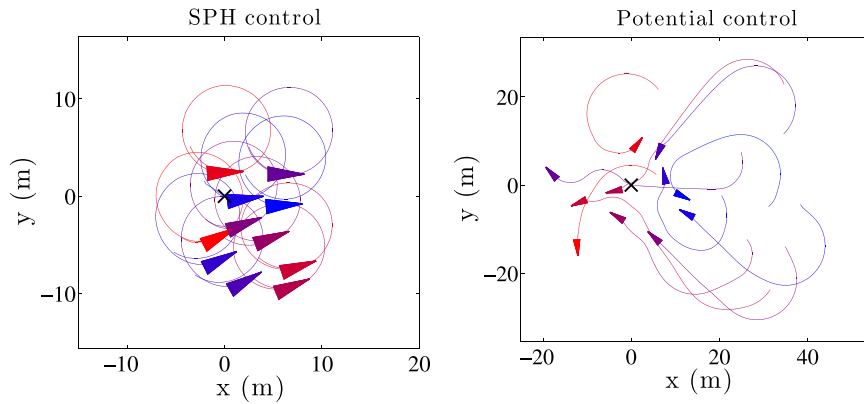


Fig. 13. The results of the SPH-based control algorithm (Left) and the potential function based control algorithm (Right) for a group of eleven vehicles and a stationary attractor particle. The viscosity term in the SPH control scheme creates a velocity consensus effect among the vehicles and results in a highly ordered swarm with good inter-vehicle spacings. Under the potential function based control scheme, the trajectories are disordered due to the lack of a consensus term, which results in inter-vehicle collisions.

vehicles tend to shorten the path in both approaches. However, the potential function based control scheme fails to maintain a coherent vehicle swarm while, on the other hand, the SPH-based method still can achieve satisfactory flocking behavior.

The performance of the two control schemes in terms of fuel usage and the minimum inter-vehicle spacing under various guidance speeds can be evaluated based on the simulation results summarized in Table 1. The relative fuel usage is calculated as

$$\eta = \frac{\text{SPH fuel usage}}{\text{Artificial potential fuel usage}}, \tag{48}$$

and the minimum inter-vehicle spacing is denoted by d_{\min}^{SPH} or $d_{\min}^{\text{Potential}}$, respectively. Similar to the stationary attractor case, when the attractor speed is smaller than the minimum vehicle speed, the potential function based approach results in slightly more energy consumption due to the disordered motion, and the minimum inter-vehicle spacing decreases significantly such that inter-vehicle collision is highly probable. Although the SPH-based control scheme consumes moderately

Table 1

Performance comparison between the SPH-based control scheme and the artificial potential based control scheme with various attractor speeds.

V_{attract} (m/s)	η	d_{\min}^{SPH}/h	$d_{\min}^{\text{Potential}}/h$
0.2	0.995	0.71	0.27
0.4	0.963	0.96	1.61
1.0	1.120	1.02	1.66
1.5	1.165	1.27	1.69

more energy compared with the potential control scheme when the attractor speed is similar to or larger than the maximum vehicle speed, it is able to maintain preferable flocking behavior and consistently moderate inter-vehicle spacings, which is highly desirable in many multi-vehicle applications.

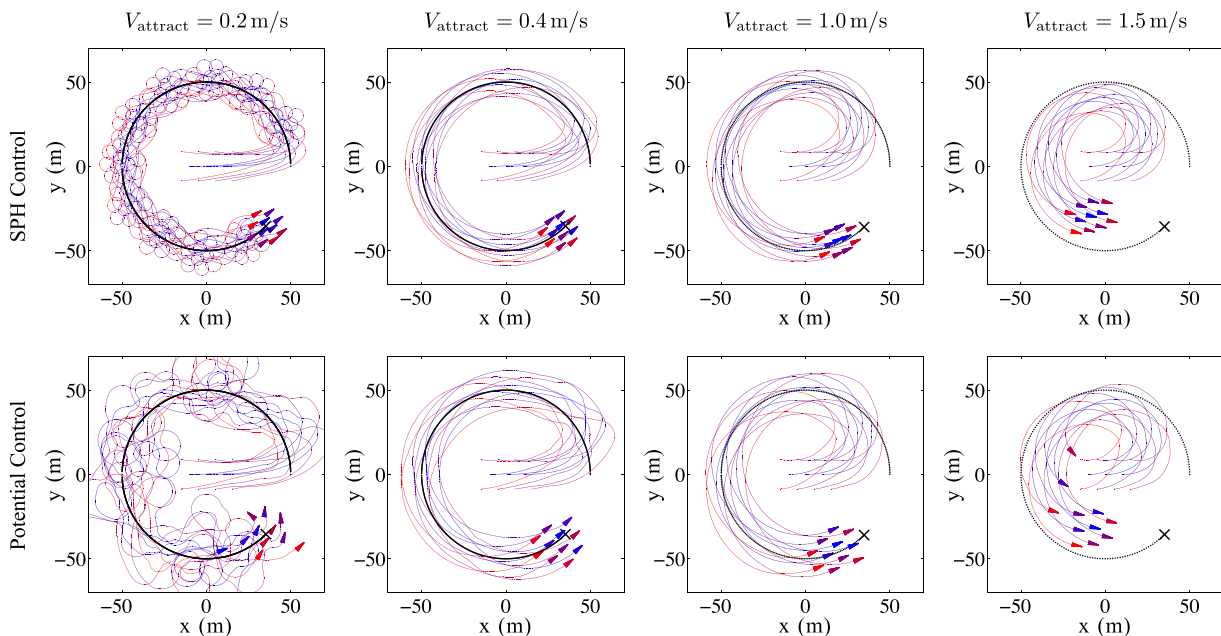


Fig. 14. Paths of eleven vehicles guided by the attracting particle with various speeds under both the SPH-based control scheme and the artificial potential based control scheme. The attractor speeds vary from 0.2 m/s, smaller than the minimum vehicle speed (0.3 m/s), to 1.5 m/s, exceeding the maximum vehicle speed (1.0 m/s).

7. Conclusions

In this paper, we proposed and analyzed a method that simultaneously addresses the multi-vehicle flocking problem and the vehicle flock guidance problem for an autonomous underwater vehicle (AUV) fleet in the presence of strong ocean flows. This method relies on computing an optimal trajectory from a starting location to a goal location under the influence of background flows that may have higher flow speeds than the agents' maximum speeds. The background flow velocity field is assumed to be predictable by ocean general circulation models. Once the optimal trajectory has been computed, vehicles can be guided approximately along this trajectory, and the vehicle fleet exhibits desirable flocking behavior. As long as the gradient of background flow velocities is small on the scale of the flock radius, it was shown that the actuation energy costs are nearly optimal for all vehicles in the flock.

For multi-vehicle flocking control and flock guidance, we proposed a control algorithm based on smoothed particle hydrodynamics (SPH) that allows the vehicle flock to behave like a fluid. Each vehicle in the flock is treated as a fluid particle, and its behavior is governed by fundamental equations of fluid motions, ensuring flock cohesion and collision avoidance through naturally obeying the underlying physics principles. We have shown a systematic method for the selection of important control parameters such that the resultant multi-vehicle behavior satisfies the essential rules of flocking, including long-range attraction, short-range repulsion, and efficient velocity matching. Additionally, choices of these parameters are based on practical constraints on vehicle dynamics such that desired vehicle velocities and accelerations generated by the control algorithm are realistically achievable. Dimensional analysis showed that the emergent flock compressibility and the velocity consensus effect are weighted by two independent parameters, the Reynolds number and the Mach number, respectively, providing an intuitive way to design the flocking behavior.

This multi-vehicle cooperation and flock guidance scheme has been tested in simulations with two different synthetic flow fields that resemble real-world flows observed in the ocean: a time-dependent double-gyre and a meandering jet, and a flow field reconstructed from ocean current model data. Flocks of up to 500 vehicles were tested and the minimum, mean, and maximum energy costs within each flock were evaluated. A least squares best fit was performed on a restricted portion of the data to verify that the energy cost scales approximately as

$$E \approx E^* + c_1 R + c_2 R^2 + c_3 R^3,$$

with E^* being the optimal trajectory cost, R being the flock radius, and c_i being constant coefficients.

For relatively small flocks such that the spatial variation of the ocean current velocity is small across the flock, the actuation energy costs of all vehicles are nearly optimal. As the flock radius increases, however, the actuation energy costs begin to grow rapidly. For very large swarms where the background flow velocity gradients are order one on the scale of the swarm radius, it is not possible to guarantee near optimality and some agents may even become separated from the swarm. This may be addressed by either decreasing the inter-vehicle spacing to decrease the flock radius or by limiting the total number of agents in a flock. The computational efficiency and the consistent performance achieved for proper swarm sizes still proved the proposed approach appealing in many practical applications.

The importance of swarm viscosity, inherently introduced by the fluid-based control scheme, was demonstrated in a series of comparisons to a generic artificial potential based control scheme that only

focuses on maintaining proper inter-agent spacings. Owing to the embedded velocity consensus effect, the proposed multi-vehicle cooperation and guidance method performed better in terms of both flocking performance and energy consumption with similar computational complexity and inter-vehicle communication requirements.

Despite the promising results, potential improvement over the current method is worth further investigation. A deeper understanding of the resultant fluid properties of the flock under the proposed flock control scheme may help discovering the inherent coupling relationship between the flock dynamics and the underlying ocean flow dynamics. Concurrently solving the underwater vehicle flock control problem and the background ocean flow dynamics is among our future research interests.

Acknowledgement

The authors would like to thank the partial support from the Office of Naval Research under grant N00014-16-1-2083 and the Air Force Research Laboratory under grant FA9550-17-1-0176.

References

- Barca, J.C., Sekercioglu, Y.A., 2013. Swarm robotics reviewed. *Robotica* 31, 345–359. (URL (http://journals.cambridge.org/article_S026357471200032X)).
- Benz, W. 1990. Smooth particle hydrodynamics: a review. In: Buchler, J. (Ed.), *The Numerical Modelling of Nonlinear Stellar Pulsations*. Vol. 302 of NATO ASI Series. Springer Netherlands, pp. 269–288. (URL (http://dx.doi.org/10.1007/978-94-009-0519-1_16)).
- Bhattacharya, R., December 2006. OPTRAGEN: a MATLAB toolbox for optimal trajectory generation. In: *Proceedings of the IEEE Conference on Decision and Control (CDC)*. San Diego, CA, USA, pp. 6832–6836.
- Brambilla, M., Ferrante, E., Birattari, M., Dorigo, M., 2013. Swarm robotics: a review from the swarm engineering perspective. *Swarm Intell.* 7 (1), 1–41. (URL (<http://dx.doi.org/10.1007/s11721-012-0075-2>)).
- Cao, Y., Yu, W., Ren, W., Chen, G., 2013. An overview of recent progress in the study of distributed multi-agent coordination. *IEEE Trans. Ind. Inform.* 9 (1), 427–438.
- Caruso, A., Paparella, F., Vieira, L., Erol, M., Gerla, M., 15–17 April 2008. The meandering current mobility model and its impact on underwater mobile sensor networks. In: *Proceedings of the IEEE Conference on Computer Communications (INFOCOM)*. Phoenix, AZ, USA, pp. 771–779. (URL (http://ieeexplore.ieee.org/xpls/abs_all.jsp?arnumber=4509648)).
- Çelikkanat, H., Şahin, E., 2010. Steering self-organized robot flocks through externally guided individuals. *Neural Comput. Appl.* 19 (6), 849–865. (URL (<http://dx.doi.org/10.1007/s00521-010-0355-y>)).
- Chassignet, E.P., Hurlburt, H.E., Metzger, E.J., Smedstad, O.M., Cummings, J.A., Halliwell, G.R., Bleck, R., Baraille, R., Wallcraft, A.J., Lozano, C., Tolman, H.L., Srinivasan, A., Hankin, S., Cornillon, P., Weisberg, R., Barth, A., He, R., Werner, F., Wilkin, J., 2009. US GODAE: global ocean prediction with the HYbrid Coordinate Ocean Model (HYCOM). *Oceanography* 2, 64–75. (URL (<http://dx.doi.org/10.5670/oceanog.2009.39>)).
- Cullen, J.M., Shaw, E., Baldwin, H.A., 1965. Methods for measuring the three-dimensional structure of fish schools. *Anim. Behav.* 13 (4), 534–543.
- Cummings, J., Smedstad, O., 2013. Variational data assimilation for the global ocean. In: Park, S.K., Xu, L. (Eds.), *Data Assimilation for Atmospheric, Oceanic and Hydrologic Applications Vol. II*. Springer, Berlin Heidelberg, 303–343. (URL (http://dx.doi.org/10.1007/978-3-642-35088-7_13)).
- DeVries, L., Paley, D., 2012. Multi-vehicle control in a strong flowfield with application to hurricane sampling. *J. Guid., Control, Dyn.* 35 (3).
- Fax, J.A., Murray, R.M., 2004. Information flow and cooperative control of vehicle formations. *IEEE Trans. Autom. Control* 49 (9), 1465–1476.
- Fossen, T.I., 2011. *Handbook of Marine Craft Hydrodynamics and Motion Control*. Wiley.
- Fossen, T.I., Sagatun, S.I., 1991. Adaptive control of nonlinear systems: a case study of underwater robotic systems. *J. Field Robot.* 8 (3), 393–412. (URL (<http://dx.doi.org/10.1002/rob.4620080307>)).
- Gazi, V., Passino, K.M., 2003. Stability analysis of swarms. *IEEE Trans. Autom. Control* 48 (4), 692–697.
- Gill, P., Murray, W., Saunders, M., 2005. SNOPT: an SQP algorithm for large-scale constrained optimization. *SIAM Rev.* 47 (1), 99–131.
- Gingold, R.A., Monaghan, J.J., 1977. Smoothed particle hydrodynamics - Theory and application to non-spherical stars. *Mon. Not. R. Astron. Soc.* 181, 375–389.
- Hsieh, M., Kumar, V., 15–19 May 2006. Pattern generation with multiple robots. In: *Proceedings of the IEEE International Conference on Robotics and Automation (ICRA)*. Orlando, FL, USA, pp. 2442–2447.

- Huhn, S., Mohseni, K., 31 May–5 June 2009. Cooperative control of a team of AUVs using smoothed particle hydrodynamics with restricted communication. In: Proceedings of the ASME International Conference on Ocean, Offshore and Arctic Engineering. Honolulu, HI, USA, pp. 531–538. (URL (<http://dx.doi.org/10.1115/OMAE2009-79869>)).
- Inanc, T., Shadden, S., Marsden, J., 8–10 June 2005. Optimal trajectory generation in ocean flows. In: Proceedings of the American Control Conference (ACC). Portland, OR, USA, pp. 674–679.
- Jadbabaie, A., Lin, J., Morse, A.S., 2003. Coordination of groups of mobile autonomous agents using nearest neighbor rules. *IEEE Trans. Autom. Control* 48 (6), 988–1001. (URL (<http://dx.doi.org/10.1109/TAC.2003.812781>)).
- Jiang, S., Jin, F.-f., Ghil, M., 1995. Multiple equilibria, periodic, and aperiodic solutions in a wind-driven, double-gyre, shallow-water model. *J. Phys. Oceanogr.* 25 (5), 764–786.
- Kelley, D.H., Ouellette, N.T., 2013. Emergent dynamics of laboratory insect swarms. *Sci. Rep.* 3.
- Khatib, O., 1986. Real-time obstacle avoidance for manipulators and mobile robots. *Int. J. Robot. Res.* 5 (1), 90–98.
- Kim, K., Ura, T., 25–30 May 2003. Fuel-optimal guidance and tracking control of AUV under current interaction. In: Proceedings of the International Offshore and Polar Engineering Conference (ISOPE). Honolulu, Hawaii, USA.
- Krieg, M., Klein, P., Hodgkinson, R., Mohseni, K., 2011. A hybrid class underwater vehicle: bioinspired propulsion, embedded system, and acoustic communication and localization system. *Mar. Technol. Soc. J.: Spec. Ed. Biomim. Mar. Technol.* 45 (4), 153–164. (URL (<http://dx.doi.org/10.4031/MTSJ.45.4.11>)).
- Krieg, M., Mohseni, K., 2010. Dynamic modeling and control of biologically inspired vortex ring thrusters for underwater robot locomotion. *IEEE Trans. Robot.* 26 (3), 542–554. (URL (<http://dx.doi.org/10.1109/TRO.2010.2046069>)).
- Krieg, M., Mohseni, K., 2015. Pressure and work analysis of unsteady, deformable, axisymmetric, jet producing cavity bodies. *J. Fluid Mech.* 769, 337–368. (URL (<http://dx.doi.org/10.1017/jfm.2015.120>)).
- Kruger, D., Stolkin, R., Blum, A., Briganti, J., 10–14 April 2007. Optimal AUV path planning for extended missions in complex, fast-flowing estuarine environments. In: Proceedings of the IEEE International Conference on Robotics and Automation (ICRA). Roma, Italy, pp. 4265–4270.
- Latombe, J.-C., 1991. *Robot Motion Planning*. Kluwer Academic Publishers, Norwell, MA, USA.
- LaValle, S.M., 2006. *Planning Algorithms*. Cambridge University Press, Cambridge, U.K.
- Leonard, N.E., Fiorelli, E., 2001. Virtual leaders, artificial potentials and coordinated control of groups. In: Proceedings of the IEEE Conference on Decision and Control (CDC). Orlando, FL, USA, 4–7 December 2001, pp. 2968–2973. (URL (<http://dx.doi.org/10.1109/2001.980728>)).
- Leonard, N.E., Paley, D.A., Lekien, F., Sepulchre, R., Fratantoni, D.M., Davis, R.E., 2007. Collective motion, sensor networks, and ocean sampling. *Proc. IEEE* 95 (1), 48–74. (URL (<http://dx.doi.org/10.1109/JPROC.2006.887295>)).
- Lermusiaux, P.F.J., Lolla, T., Haley, P.J., Yigit, K., Ueckermann, M.P., Sondergaard, T., Leslie, W.G., 2016. Science of autonomy: time-optimal path planning and adaptive sampling for swarms of ocean vehicles. In: Dhanak, M.R., Xiros, N.I. (Eds.), *Springer Handbook of Ocean Engineering*. Springer International Publishing, 481–498. (URL (http://dx.doi.org/10.1007/978-3-319-16649-0_21)).
- Lipinski, D., Mohseni, K., 2010. Cooperative control of a team of unmanned vehicles using smoothed particle hydrodynamics. In: Proceedings of the AIAA Guidance, Navigation, and Control Conference. No. 2010–8316. Toronto, Canada. 2–5 August 2010. (URL (<http://dx.doi.org/10.2514/6.2010-8316>)).
- Lipinski, D., Mohseni, K., 2011. A master-slave fluid cooperative control algorithm for optimal trajectory planning. In: Proceedings of the IEEE International Conference on Robotics and Automation (ICRA). Shanghai, China, 9–13 May 2011, pp. 3347–3351. (URL (<http://dx.doi.org/10.1109/ICRA.2011.5980401>)).
- Lipinski, D., Mohseni, K., 2013. Nearly fuel-optimal trajectories for vehicle swarms in open domains with strong background flows. In: Proceedings of the IEEE/RSJ International Conference on Intelligent Robots and Systems (IROS). Tokyo, Japan, 3–7 November 2013, pp. 3847–3842. (URL (<http://dx.doi.org/10.1109/IROS.2013.6696905>)).
- Liu, G.R., Liu, M.B., 2003. *Smoothed Particle Hydrodynamics: A Meshfree Particle Method*. World Scientific, Hackensack, NJ, USA.
- Lolla, T., Ueckermann, M.P., Yigit, K., Haley, P.J., Lermusiaux, P. F.J., 2012. Path planning in time dependent flow fields using level set methods. In: Proceedings of the IEEE International Conference on Robotics and Automation (ICRA). St. Paul, MN, USA, 14–18 May 2012, pp. 166–173.
- Lucy, L.B., 1977. A numerical approach to the testing of the fission hypothesis. *Astron. J.* 82, 1013–1024.
- Major, P.F., Dill, L.M., 1978. The three-dimensional structure of airborne bird flocks. *Behav. Ecol. Sociobiol.* 4 (2), 111–122.
- Mallory, K., Hsieh, M.A., Forgoston, E., Schwartz, I.B., 2013. Distributed allocation of mobile sensing swarms in gyre flows. *Nonlinear Process. Geophys.* 20 (5), 657–668.
- Monaghan, J.J., 1992. Smoothed particle hydrodynamics. *Annu. Rev. Astron. Astrophys.* 30, 543–574. (URL (<http://dx.doi.org/10.1146/annurev.aa.30.090192.002551>)).
- Monaghan, J.J., 1994. Simulating free surface flows with SPH. *J. Comput. Phys.* 110 (2), 399–406. (URL (<http://www.sciencedirect.com/science/article/pii/S0021999184710345>)).
- Monaghan, J.J., 2005. Smoothed particle hydrodynamics. *Rep. Progress. Phys.* 68 (8), 1703.
- Monaghan, J.J., 2012. Smoothed particle hydrodynamics and its diverse applications. *Annu. Rev. Fluid Mech.* 44 (1), 323–346. (URL (<http://dx.doi.org/10.1146/annurev-fluid-120710-101220>)).
- Moreau, L., 2005. Stability of multiagent systems with time-dependent communication links. *IEEE Trans. Autom. Control* 50 (2), 169–182.
- Morris, J.P., Fox, P.J., Zhu, Y., 1997. Modeling low Reynolds number incompressible flows using SPH. *J. Comput. Phys.* 136 (1), 214–226. (URL (<http://www.sciencedirect.com/science/article/pii/S0021999197957764>)).
- Morrow, J.E., 1948. Schooling behavior in fishes. *Q. Rev. Biol.* 23 (1), 27–38.
- Naval Research Laboratory, 2015. Real-time 1/25 ° Gulf of Mexico HYCOM. (URL (<http://www7320.nrlssc.navy.mil/hycomGOM/>)).
- Olfati-Saber, R., 2006. Flocking for multi-agent dynamic systems: algorithms and theory. *IEEE Trans. Autom. Control* 51 (3), 401–420. (URL (<http://dx.doi.org/10.1109/TAC.2005.864190>)).
- Olfati-Saber, R., Murray, R.M., 2004. Consensus problems in networks of agents with switching topology and time-delays. *IEEE Trans. Autom. Control* 49 (9), 1520–1533.
- Pac, M., Erkmén, A., Erkmén, I., 2007. Control of robotic swarm behaviors based on smoothed particle hydrodynamics. In: Proceedings of the IEEE/RSJ International Conference on Intelligent Robots and Systems (IROS). San Diego, CA, USA, 29 October–2 November 2007, pp. 4194–4200.
- Paley, D., Zhang, F., Leonard, N., 2008. Cooperative control for ocean sampling: the glider coordinated control system. *IEEE Trans. Control Syst. Technol.* 16, 735–744.
- Paley, D. A., 2007. *Cooperative Control of Collective Motion for Ocean Sampling with Autonomous Vehicles* (Ph.D. thesis). Princeton University, Princeton, NJ, USA.
- Perkinson, J. R., Shafai, B., 2005. A decentralized control algorithm for scalable robotic swarms based on mesh-free particle hydrodynamics. In: Proceedings of the IASTED International Conference on Robotics and Applications. Cambridge, MA, USA, 1–3 November 2005, pp. 1–6.
- Petres, C., Pailhas, Y., Patron, P., Petitot, Y., Evans, J., Lane, D., 2007. Path planning for autonomous underwater vehicles. *IEEE Trans. Robot.* 23 (2), 331–341.
- Pimenta, L.C.A., Michael, N., Mesquita, R.C., Pereira, G.A.S., Kumar, V., 2008. Control of swarms based on hydrodynamic models. In: Proceedings of the IEEE International Conference on Robotics and Automation (ICRA). Pasadena, CA, USA, 19–23 May 2008, pp. 1948–1953.
- Pimenta, L.C.A., Pereira, G.A.S., Michael, N., Mesquita, R.C., Bosque, M.M., Chaimowicz, L., Kumar, V., 2013. Swarm coordination based on smoothed particle hydrodynamics technique. *IEEE Trans. Robot.* 29, 383–399.
- Ren, W., Beard, R.W., Atkins, E.M., 2005. A survey of consensus problems in multi-agent coordination. In: Proceedings of the American Control Conference (ACC). Portland, OR, USA, 8–10 June 2005, pp. 1859–1864.
- Reynolds, C.W., 1987. Flocks, herds and schools: A distributed behavioral model. In: Proceedings of the 14th Annual Conference on Computer Graphics and Interactive Techniques (SIGGRAPH). vol. 21. ACM, New York, NY, USA, pp. 25–34.
- Rhoads, B., Mezic, I., Poje, A., 2010. Minimum time feedback control of autonomous underwater vehicles. In: Proceedings of the IEEE Conference on Decision and Control (CDC). Atlanta, Georgia, USA, 15–17 December 2010, pp. 5828–5834.
- Rubenstein, M., Cornejo, A., Nagpal, R., 2014. Programmable self-assembly in a thousand-robot swarm. *Science* 345 (6198), 795–799. (URL (<http://www.sciencemag.org/content/345/6198/795.abstract>)).
- Sabatini, M., Palmerini, G., Gasbarri, P., 2014. Control laws for defective swarming systems. In: Proceedings of the 2nd IAA Conference on Dynamics and Control of Space Systems (DyCoSS). Rome, Italy, pp. 749–768.
- Sabatini, L., Chopra, N., Secchi, C., 2013. Decentralized connectivity maintenance for cooperative control of mobile robot systems. *Int. J. Robot. Res.* 32 (12), 1411–1423. (URL (<http://ijr.sagepub.com/content/32/12/1411.abstract>)).
- Samelson, R., 1992. Fluid exchange across a meandering jet. *J. Phys. Oceanogr.* 22 (4), 431–444.
- Shadden, S.C., Lekien, F., Marsden, J.E., 2005. Definition and properties of Lagrangian coherent structures from finite time Lyapunov exponents. *Phys. D* 212 (3–4), 271–304. (URL (<http://dx.doi.org/10.1016/j.physd.2005.10.007>)).
- Shang, Y., Bouffanais, R., 2014. Influence of the number of topologically interacting neighbors on swarm dynamics. *Sci. Rep.* 4.
- Shaw, A., Mohseni, K., 2011. A fluid dynamic based coordination of a wireless sensor network of unmanned aerial vehicles: 3-d simulation and wireless communication characterization. *IEEE Sens. J. Spec. Issue Cogn. Sens. Netw.* 11 (3), 722–736. (URL (<http://dx.doi.org/10.1109/JSEN.2010.2064294>)).
- Shchepetkin, A.F., McWilliams, J.C., 2005. The regional oceanic modeling system (ROMS): a split-explicit, free-surface, topography-following-coordinate oceanic model. *Ocean Model.* 9 (4), 347–404. (URL (<http://www.sciencedirect.com/science/article/pii/S1463500304000484>)).
- Song, Z., Mazzola, C., Schwartz, E., Finlaw, J., Chen, R., Krieg, M., Mohseni, K., 2016. A compact autonomous underwater vehicle with cephalopod-inspired propulsion. *Mar. Technol. Soc. J.* 50 (5), 88–101. (URL (<http://dx.doi.org/10.4031/MTSJ.50.5.9>)).
- Spears, W.M., Spears, D.F., 2012. *Physicmimetics: Physics-Based Swarm Intelligence*. Springer, Berlin, Heidelberg.
- Spears, W.M., Spears, D.F., Heil, R., Kerr, W., Hettiarachchi, S., 2005. An overview of physicmimetics. In: Şahin, E., Spears, W. (Eds.), *Swarm Robotics*. Vol. 3342 of

- Lecture Notes in Computer Science. Springer Berlin Heidelberg, pp. 84–97. (URL (http://dx.doi.org/10.1007/978-3-540-30552-1_8)).
- Speich, S., Dijkstra, H., Ghil, M., 1995. Successive bifurcations in a shallow-water model applied to the wind-driven ocean circulation. *Nonlinear Process. Geophys.* 2 (3/4), 241–268. (URL (<http://www.nonlin-processes-geophys.net/2/241/1995/>)).
- Speich, S., Ghil, M., 1994. Interannual variability of the mid-latitude oceans: a new source of climate variability. *Sist. Terra* 3 (3), 459.
- Thomasson, P., Woolsey, C., 2013. Vehicle motion in currents. *IEEE J. Ocean. Eng.* 38 (2), 226–242.
- Toner, J., Tu, Y., 1998. Flocks, herds, and schools: a quantitative theory of flocking. *Phys. Rev. E* 58 (October), 4828–4858. (URL (<http://link.aps.org/doi/10.1103/PhysRevE.58.4828>)).
- Vicsek, T., Zafeiris, A., 2012. Collective motion. *Phys. Rep.* 517 (3–4), 71–140. (URL (<http://www.sciencedirect.com/science/article/pii/S0370157312000968>)).
- Witt, J., Dunbabin, M., 2008. Go with the flow: optimal AUV path planning in coastal environments. In: *Proceedings of the Australian Conference on Robotics and Automation (ACRA)*. Canberra, Australia, 3–5 December 2008.
- Xu, Y., Mohseni, K., 2014. Bioinspired hydrodynamic force feedforward for autonomous underwater vehicle control. *IEEE/ASME Trans. Mechatron.* 19 (4), 1127–1137. (URL (<http://dx.doi.org/10.1109/TMECH.2013.2271037>)).
- Zhang, F., Fratantoni, D.M., Paley, D.A., Lund, J.M., Leonard, N.E., 2007. Control of coordinated patterns for ocean sampling. *Int. J. Control* 80 (7), 1186–1199. (URL (<http://dx.doi.org/10.1080/00207170701222947>)).
- Zhao, S., Ramakrishnan, S., Kumar, M., 2011. Density-based control of multiple robots. In: *Proceedings of the American Control Conference (ACC)*. San Francisco, CA, USA, 29 June–1 July 2011, pp. 481–486.